UNIVERSITA' DEGLI STUDI DI FERRARA
FACOLTA' DI INGEGNERIA

Corso di Laurea in Ingegneria e Tecnologie per le Telecomunicazioni e l'Elettronica

DEVELOPMENT OF THE SYSTEM TEST FOR THE LHC TUNE MEASUREMENT AND ABORT GAP MONITORING

Tesi di Laurea di:
Barbara Beccati

Primo Relatore:
Prof. Gianluca Mazzini

Correlatore:
Dott. Andrea Boccardi

Secondo Relatore:
Prof. Gianluca Setti

Terzo Relatore:
Prof. Velio Tralli

"Be the change that you want to see in the world.",
Mahatma Gandhi

Introduzione

Il CERN, Centro Europeo per la Ricerca Nucleare, è uno dei più grandi centri di ricerca al mondo. Al CERN vengono utilizzate le tecnologie più innovative per studiare i componenti base della materia: acceleratori di particelle e detectors. I primi accelerano fasci di particelle ad alta energia per realizzare collisioni tra i fasci stessi o con altri target. I secondi vengono utilizzati per osservare e registrare i risultati di queste collisioni.

LHC, Large Handron Collider, è l'acceleratore di particelle più grande e potente mai realizzato dall'uomo, progettato per far collidere protoni ad un'energia di 14 TV, mai raggiunta fino ad ora in laboratorio. È costruito all'interno di un tunnel sotterraneo lungo 27 km situato al confine tra la Francia e la Svizzera.

Io, nell'ambito del progetto IUSS-Ferrara, ho collaborato con i membri della sezione AB-BI del CERN: Accelerator Beam - Beam Instrumentation. La mia tesi è il frutto di questa collaborazione.

LHC è un sincrotrone: in questo tipo di acceleratori sono presenti alcuni magneti con il compito di curvare la traiettoria delle particelle ed altri (quadrupoli) atti ad impedire la fuoriscita di particelle dalla traiettoria stessa. Le particelle, attraversando questo pattern di magneti, oscillano: tali oscillazioni sono chiamate oscillazioni Betatron. Il numero di oscillazioni compiute nel periodo di rivoluzione è detto Betatron Tune.

La prima parte del mio progetto e' relativa al Tune e al suo sistema di misura con particolare enfasi sulla strumentazione utilizzata perche' parte di essa e' stata impiegata in diverse fasi del mio lavoro.

La capacità di misurare il Tune è infatti importante in molti tipi di diagnostica. Al CERN è stato sviluppato un sistema di misurazione del Tune in banda base (BBQ) in cui il segnale digitale viene processato da una FPGA integrata in una scheda VME chiamata DAB (Digital Acquisition Board). Questa scheda è provvista di una memoria detta di post mortem che viene utilizzata per memorizzare i dati relativi agli ultimi istanti di "vita" del fascio nel caso in cui si verifichi una sua perdita accidentale.

La parte del mio progetto relativamente a questo argomento ha come scopo la verifica del corretto funzionamento della memoria di post mortem. Per verificare ciò ho sviluppato un software in LabVIEW per poter interagire con la memoria di post mortem stessa e ho realizzato alcuni test, simulando opportunamente eventi di perdita del fascio di particelle.

La seconda parte del mio elaborato è relativa all'Abort Gap. LHC è caratterizzato da una grande quantità di energia accumulata: per questo è stato sviluppato al CERN uno speciale metodo di espulsione dell'energia. Affinchè esso funzioni correttamente è necessario avere un intervallo di $3.3\ \mu s$ durante il quale non si abbiano particelle nel pattern fascio. Questo intervallo di tempo è chiamato Abort Gap.

Per monitorare la presenza di particelle cariche nell'abort gap di LHC si è scelto di misurare la radiazione sincrotronica emessa dalle particelle stesse. Il sistema che permette di catturare la radiazione sincrotronica di LHC è chiamato **telescope**. Il sistema di monitoraggio dell'abort gap in LHC deve quindi analizzare la radiazione sincrotronica emessa dal fascio: il dispositivo usato per misurare quest'ultima è un MCP-PMT (MicroChannel Plate PhotoMultiplier). Quest'ultimo puo' essere descritto come un insieme di amplificatori di elettroni miniaturizzati disposti parallelamente l'uno all'altro.

La soluzione adottata al CERN per analizzare il segnale fornito dal PMT prevede il riutilizzo della scheda DAB (utilizzata per molteplici scopi, ad esempio la misurazione del tune) equipaggiata con una scheda chiamata IBMS mezzanine.

La mia parte di progetto relativamente a questo argomento ha come obiettivi:

- permettere all'utente, tramite un'iterfaccia software, il monitoraggio dell'abort gap. Ho quindi sviluppato un software in LabVIEW per il controllo della FPGA integrata nella DAB, responsabile del processamento del segnale proveniente dal PMT.

- costruire un setup per poter testare l'applicazione software in quanto non si dispone del fascio di particelle di LHC e quindi non è possibile analizzare la radiazione sincrotronica da esse emessa. E' stato perciò un mio compito costruire questo setup, utilizzando un generatore di impulsi ed un fotodiodo per generare la radiazione luminosa in ingresso al PMT e sviluppando un software per il controllo via GPIB del generatore.

- calibrare e analizzare le performance, in termini di rapporto segnale rumore, di questo sistema per poter confrontare i risultati da me ottenuti con quelli ricavati, usando lo stesso setup, all'interno del tunnel LHC al fine di riscontrare eventuali anomalie nella catena di acquisizione del segnale.

Ho quindi realizzato le misure necessarie utilizzando il mio software per il monitoraggio dell'abort gap e ho sviluppato due diverse applicazioni, una per calibrare gli integratori della scheda mezzanine ed una seconda per analizzare il livello di rumore presente nel sistema.

Gli argomenti da me affrontati durante la mia collaborazione al CERN vengono così presentati in questo elaborato:

- nel primo capitolo descrivo i componenti fondamentali di un sincrotrone e di LHC, il suo layout e la struttura del fascio, nonchè il sistema di iniezione del fascio in LHC;
- nel secondo capitolo definisco il betatron tune, descrivo il sistema di misura di quest'ultimo sviluppato al CERN e il software ed il test realizzato relativamente alla memoria di post mortem;
- nel terzo capitolo definisco l'Abort Gap di LHC e la sua funzione oltre a descrivere come questo viene monitorato attraverso l'analisi della radiazione sincrotronica emessa dalle particelle cariche che lo popolano;
- nel quarto capitolo descrivo la catena di acquisizione del segnale per il monitoraggio dell'abort gap, sottolineando quali componenti sono stati riutilizzati e le ragioni di ciò;
- nel quinto capitolo descrivo come vengono processati i dati aquisiti, il setup usato in laboratorio, i software sviluppati per il monitoraggio dell'abort gap e l'analisi dei dati, le misure e la calibrazione eseguite;
- nel sesto capitolo, infine, riporto le conclusioni del mio lavoro.

Introduction

CERN, the European Organization for Nuclear Research, is one of the largest and most respected centres for scientific research all over the world. It deals with fundamental physics, finding out what the Universe is made of and how it works. At CERN, the world's largest and most complex scientific instruments are used to study the basic constituents of matter - the fundamental particles. By studying what happens when these particles collide, physicists learn about the laws of Nature. The instruments used at CERN are particle accelerators and detectors. Accelerators boost beams of particles to high energies before they are collided against each other or with stationary targets. Detectors observe and record the results of these collisions.

The Large Hadron Collider (LHC) is the largest accelerator in the world and it will collide opposing beams of $7\ \mathrm{TV}$ protons together. It is built inside a 27 km tunnel on the border between France and Switzerland.

Within the framework of the project IUSS- Ferrara, I collaborated with the members of the AB-BI section at CERN: Accelerator Beam - Beam Instrumentation. My degree thesis is the result of this cooperation. My project is made of two sections, one for each themes analyzed during this year at CERN: the first one concerns the Tune, the second one is about the Abort gap.

LHC is a synchrotron, an accelerator using dipole magnets to bending and quadrupole magnets to transverse focusing. Passing through this pattern of magnets, particles make oscillations. We refer to these ones as Betatron oscillations. The number of such oscillations/turn is called Tune.

The ability to measure the tune is important for many kinds of diagnostic. In the base band tune (BBQ) measurement system developed at CERN the signal is digitized with a 24bit audio codec and is processed in the FPGA of a VME board (DAB, Digital Acquisition Board). The DAB is equipped with a post mortem memory: its function is to save the last received data before a beam loss.

My goal in this subject was to verify the correct working of the post mortem memory. In order to do it, I developed a LabVIEW software to interface with this memory and I performed some tests properly simulating events of beam loss.

The second part of my project is about the abort gap monitoring. The rings of LHC are characterized by a lot of accumulative energy (around 350 MJ/beam) that implies being careful with accidental beam losses. In order to manage such a huge amount of energy, a special expulsion system was developed to safely extract the protons from the ring. It is necessary to have a gap of $3.3\ \mu s$ (which is exactly the time that kickers) free of charge: it is called the abort gap.

To detect the presence of charged particles in the abort gap of the LHC, we measure the synchrotron radiation they emit with a synchrotron light extraction system called telescope. The collected light is converted into voltage signal using a MCP-PMT and digitalized to perform the further processing.

The CERN solution chosen to analyze the PMT output signal uses the DAB board (designed to be a basic multifunction element for various application, like the tune measurement). This board is composed by an Altera Stratix FPGA which processes the digital data for the IBMS mezzanine.

In this framework, my targets consist in:

- to allow the user to monitor the abort gap. I developed a LabVIEW software to control the FPGA of the DAB which is responsible for the processing of the signal coming from the PMT.

- to develop a testing setup for the acquisition chain because I could not use the synchrotron light of LHC. Therefore I developed this testing setup using a pulse delay generator to control a photodiode in order to generate the light input for the PMT. Moreover I developed a software to remotely control the generator.

- to calibrate the system and to analyze its noise performance, in order to compare my results with the ones coming from the same acquisition chain located in the tunnel of LHC. Therefore I performed my measurements using my abort gap monitoring tool; I also developed two different applications, to calibrate the integrators in the mezzanine and to analyze the noise level in the system, respectively.

The outline of my project is:

- the first chapter is about the main components of a synchrotron accelerator and of LHC, its layout, its beam structure and its injection chain;

- the second chapter is about the betatron tune and its measurment technique developed at CERN. I also talk about the post mortem data and I described my software and my tests for the post mortem memory;

- the third chapter is about the LHC abort gap; I also describe how to montor it, measuring the synchrotron light emitted by the charged particles which populate it;
- the fourth chapter is about the abort gap acquisition chain, with focusing on the reason to use a VME solution;
- the fifth chapter is about the data treatment: I describe the testing setup, the developed software tools and my measurement results.
- the sixth chapter presents my conclusions.

Contents

List of Figures

Chapter 1

Large Hadron Collider

1.1 Accelerator Basic Principles

A particle accelerator is a device that uses electric fields to propel electrically-charged particles to high speeds and magnetic fields to contain them. Electron gun for an ordinary television set is a simple form of accelerator.

There are two basic types of accelerators: linear accelerators [1] and circular accelerators.

The term circular accelerator refers to any machine in which beams describe a closed orbit. Beam orbits are often not true circles; for instance, large synchrotrons are composed of alternating straight and curved sections.

In any kind of accelerator there is one path - the design orbit - on which ideally all particles should move. If this design orbit is curved, **bending** forces are needed. In reality, most particles of the beam deviate slightly from the design orbit. In order to minimize these deviations and to keep the beam size small, **focusing** forces are required. Both bending and focusing forces can be accomplished with magnetic fields (see figure 1.1).

Synchrotrons are the present standard circular accelerators for particle physics research. An ultra-hight-vacuum chamber for beam transport forms a closed loop. Arc sections may be interrupted by straight sections to facilitate beam injection, beam exctraction and experiments. Acceleration is provided by electrical fields within a resonanting structure, fed by a RF power source [1].

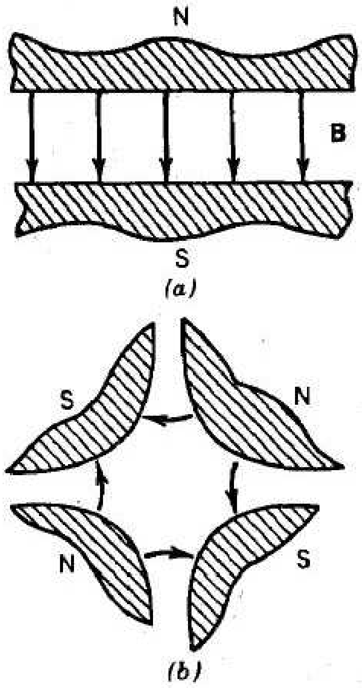

Figure 1.1: Dipole and Quadrupole Magnets.

The bunch structure of a modern accelerator is a direct consequence of the radio frequency (RF) of the accelerating fields. Particles can only be accelerated when the RF field has the correct orientation when particles pass through an accelerating cavity, which happens at well specified moments during an RF cycle.

The global arrangement of magnets around the synchrotron is called **focusing lattice**. We call **focusing cell** the smallest element of periodicity in a focusing system.

The most common example of focusing cell is the FODO cell (see figure 1.2). It consists of a focusing quadrupole (QF) and a defocusing quadrupole (QD). A QF focuses the beam in the horizontal plane and defocusing the beam in the vertical one; a QD does the opposite. We can think quadrupoles magnets as thin lenses, which are concave in one plane and convex in the other. An alterning series of focusing and defocusing lenses leads up to an overall focusing because the focusing lenses are, on the average, traversed at larger distance from the central axis than the defocusing ones [4] (see figure 1.3). This focusing technique

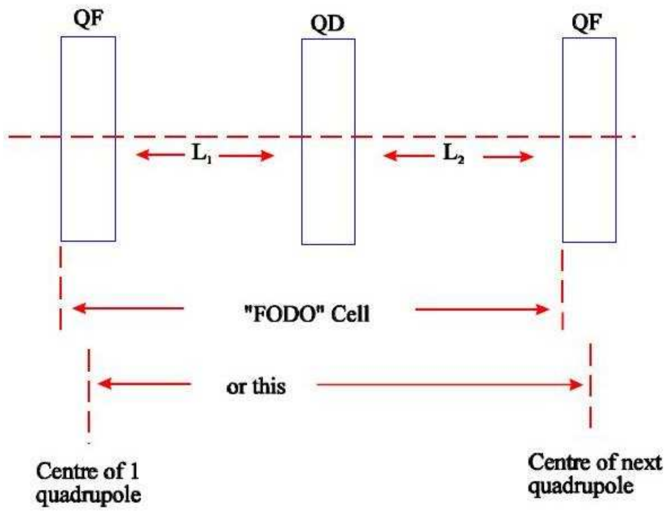

Figure 1.2: Layout of a FODO cell

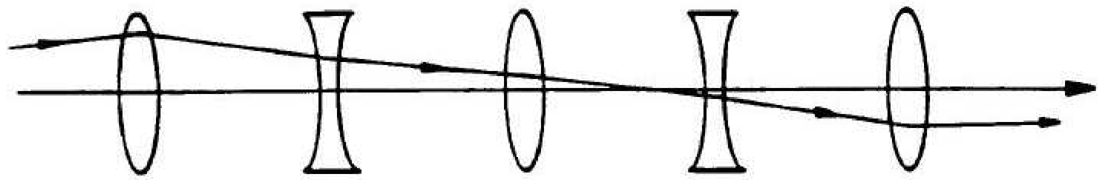

Figure 1.3: Alternating -gradient focusing

is called **alternating-gradient focusing**.

1.2 LHC

LHC stands for Large Hadron Collider. Large due to its size (approximately $27\ \mathrm{km}$ in circumference); Hadron because it accelerates proton or ions, which are hadronic particles, and Collider because these particles form beams travelling in opposite directions, which collide at four points around the machine's circumference. The size of an accelerator is related to the maximum energy obtainable. In the case of a circular collider, this depends on the radius of the machine and the strength of the dipole magnetic field that keeps particles on their orbits.

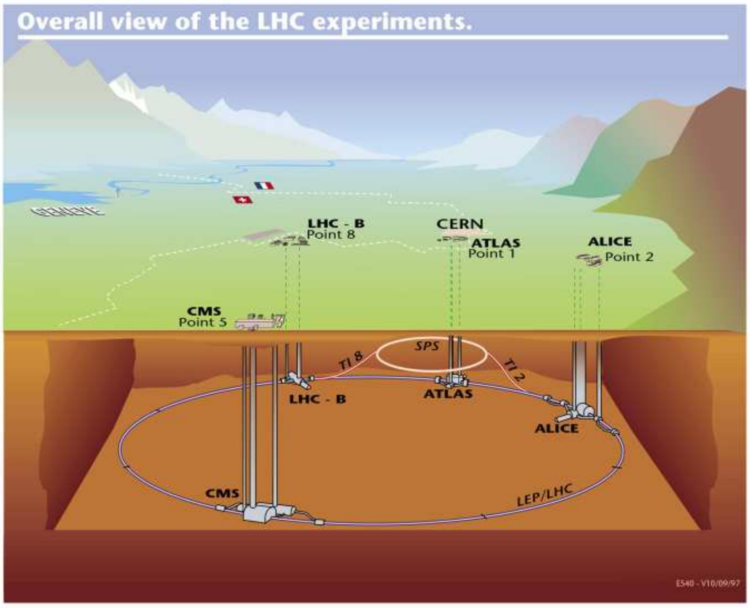

Figure 1.4: LHC underground

A collider has a big advantage over fixed target experiments. When two beams collide, the energy of the collision is the sum of the energies of the two beams. The two beams travel in opposite directions around the ring in individual beam pipes. Protons beams intersect at different points distributed along the ring. Proton-protron interactions are studied by detectors located near the intersection points (see figure 1.4). There are six experiments installed at the LHC: A Large Ion Collider Experiment (ALICE), ATLAS (A Toroidal LHC ApparatuS), the Compact Muon Solenoid (CMS), the Large Handron Collider beauty (LHCb) experiment, the Large Handron Collider forward (LHCf) and the TOTal Elastic and diffractive cross section Measurement (TOTEM) [13].

1.2.1 The important parameters

Scientists build colliders to probe elementary particles costituting matter. Each of these particles are only observable above a specific energy threshold and the ability to observe them increases with energy. This means that for high energy physicists the most important parameters are the beam energy and the number of interesting collision. To quantify the perfomance of a collider, a quantity called **luminosity** has been introduced. It depends on the number of particles in each bunch, the frequency of complete turns around the ring, the number of bunches and the beam cross-section. In fact we can express the luminosity as:

$$L = fn\frac{N_1 N_2}{A} \tag{1.1}$$

where L is the luminosity, n is the number of bunches in one beam in the storage ring, N_i is the number of particles in each bunch and A is the cross section of the beams [5].

The other important parameter is the energy. The protons will each have an energy of $7\ \mathrm{TeV}$, giving a total collision energy of $14\ \mathrm{TeV}$: these energies have never been reached before in a laboratory.

1.2.2 The main components

In an accelerator, particles circulate in a vacuum tube and are manipulated using electromagnetic devices. Dipole magnets keep the particles in their nearly circular orbits, quadrupole magnets focus the beam, and accelerating cavities are electromagnetic resonators that accelerate particles and then keep them at a constant energy by compensating for energy losses. LHC cavities deliver radiofrequency (RF) power to the beam during acceleration to the top energy and keep the 2808 proton bunches (each bunch contains 10^{11} protons) tightly bunched to ensure high luminosity at the collision points and hence, maximize the number of collisions.

1.2.3 Layout and beam structure of LHC

The LHC is designed with eight arc sections and eight straight sections. Each of those arcs consists of 23 identical cells. These cells are made up of six dipoles and two quadrupoles. Dipoles are used in order to deflect the beam while quadrupoles are used as magnetic lens to focus the beam.

The protons of the LHC circulate around the ring in well-defined bunches. The bunch size is not constant around the ring. Each bunch, as it circulates around the LHC, gets squeezed and expanded - for instance it gets squeezed as much as possible around the interaction points to increase the probability of a collision. Bunches of particles measure a few centimeters long and a millimeter wide when they are far from a collision point. However, as they approach the collision points, their width is squeezed to about $16\ \mu m$(a human hair is about $50\ \mu m$ thick) to allow for a greater chance of proton - proton collisions. Increasing the number of bunches is one of the ways to increase luminosity in a machine.

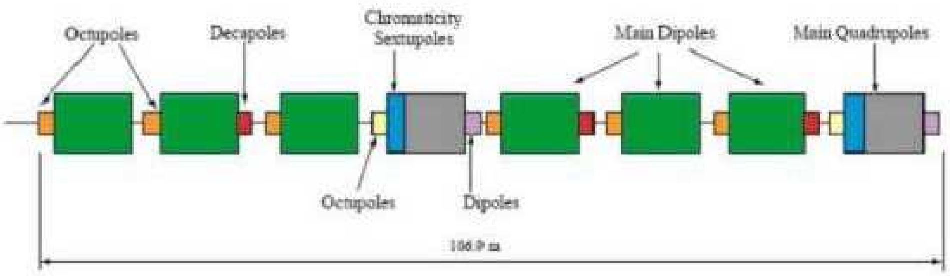

Figure 1.5: LHC magnets.

In the LHC, under nominal operation conditions, each proton beam has 2808 bunches, with each bunch containing about 10^{11} protons.

1.2.4 LHC Injection Complex

The accelerator complex at CERN is a succession of machines with increasingly higher energies. Each machine injects the beam into the next one, which takes over to bring the beam to an even higher energy, and so on. In the LHC - the last element of this chain - each particle beam is accelerated up to $7\ \mathrm{TeV}$. The brief story of a proton accelerated through the accelerator complex of CERN is as follows:

- Protons are injected into the PS Booster (PBS) at an energy of $50\ \mathrm{MeV}$ from Linac2.
- The booster accelerates them to $1,4\ \mathrm{GeV}$.
- The beam is then fed to the Proton Synchrotron (PS) where it is accelerated up to $25\ \mathrm{GeV}$.
- Protons are sent to the Super proton Synchrotron (SPS) where they are accelerated to $450\ \mathrm{GeV}$.
- They are finally transferred to the LHC where they are accelerated to their nominal $7\ \mathrm{TeV}$.

1.3 CERN/BI standard solution for Data Acquisition

LHC is a very complex machine, as well as the related measurement systems. To make the system maintenance easier, a standard system for the data acquisition (from the digitalization stage) was developed by AB/BI section. It opted for a VME - based acquisition system controlled by a linux-based power PC. This system encompasses the Beam OBseRvation system (BOBR) and the Digital Acquisition Board (DAB). The BOBR is a VME format card, designed to interface a VME crate with up two different TTC (Timing, Trigger and Control system) and to provide the timing signals (including the 40MHz bunch clock)in a fully synchronized way to LHC experiment areas.

The DAB64X (see figure 1.7) developed by TRIUMF for CERN applications is a VME board with:

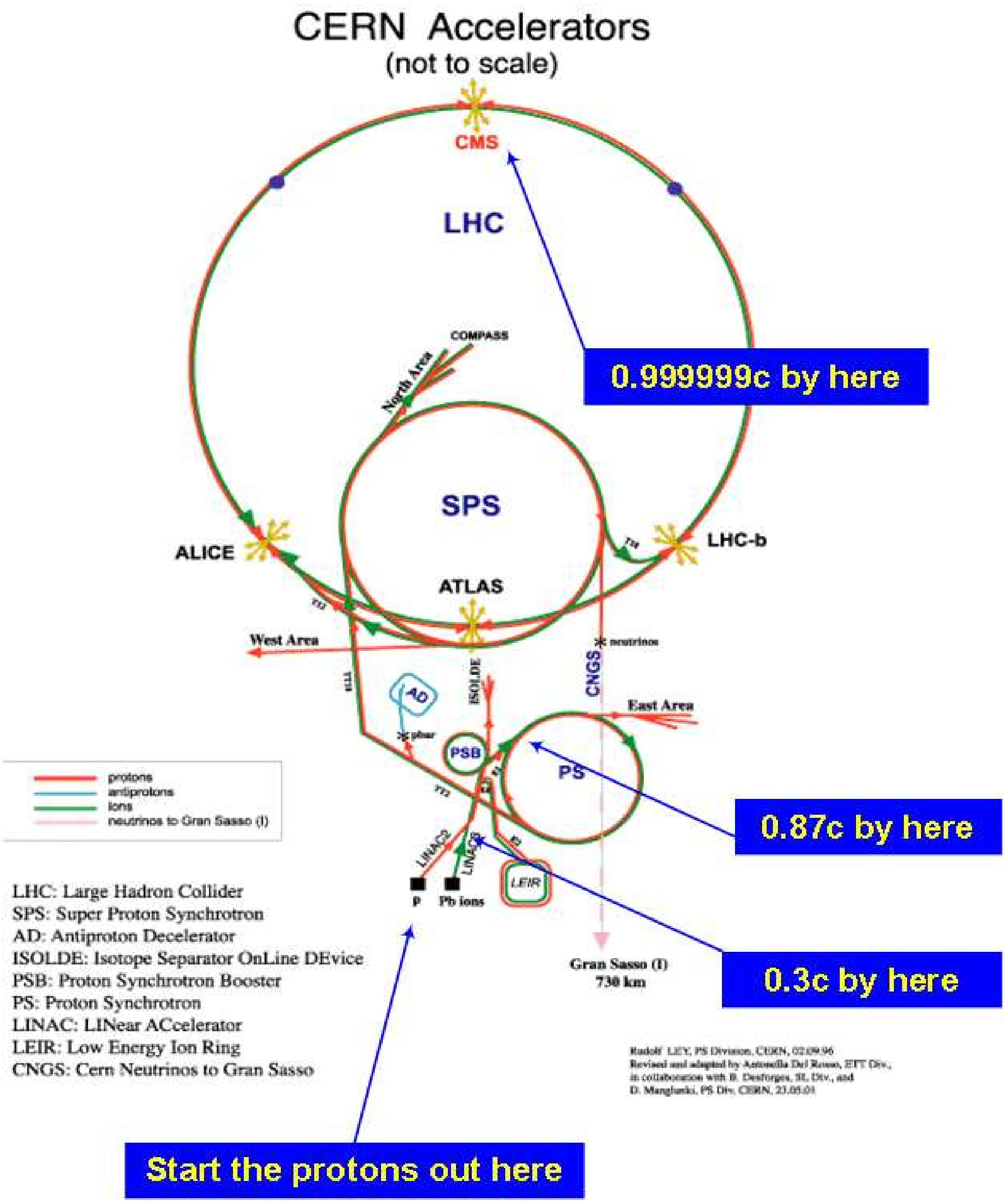

Figure 1.6: The CERN Accelerators Complex

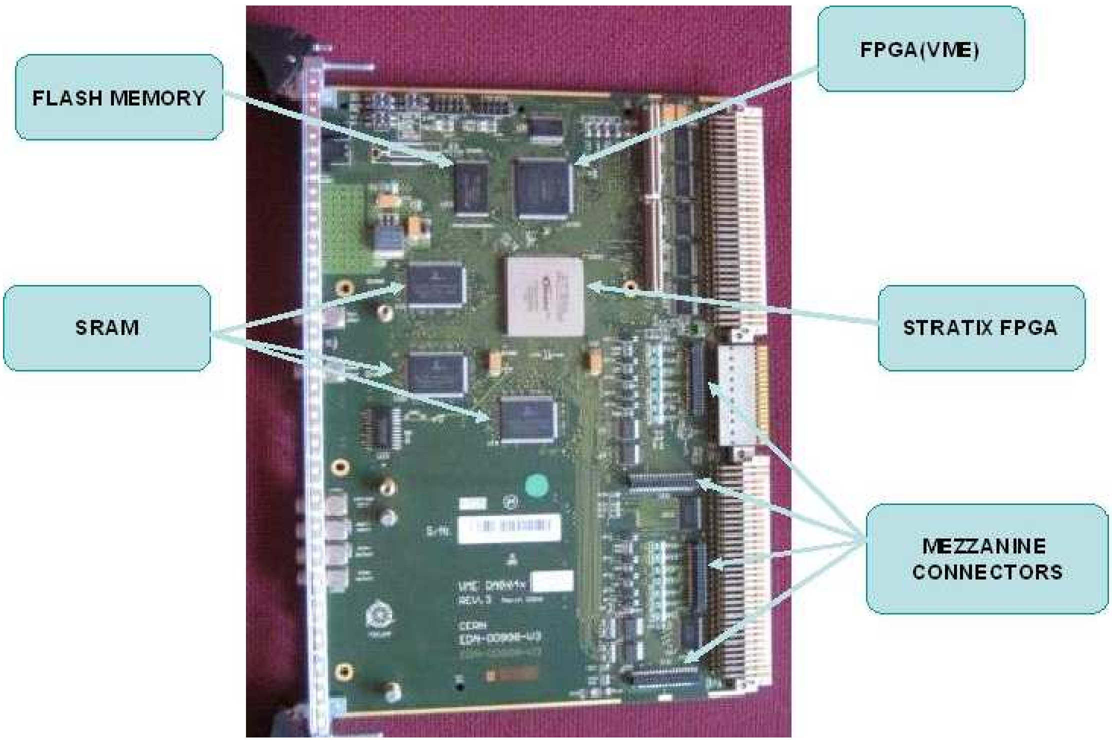

Figure 1.7: DAB64X

- two FPGAs, one of them (STRATIX) for applications
- two mezzanine board locations that can be used to customize the board to the specific need of the instrument.

Chapter 2

Tune Monitoring

2.1 Betatron envelopes and Tune definition

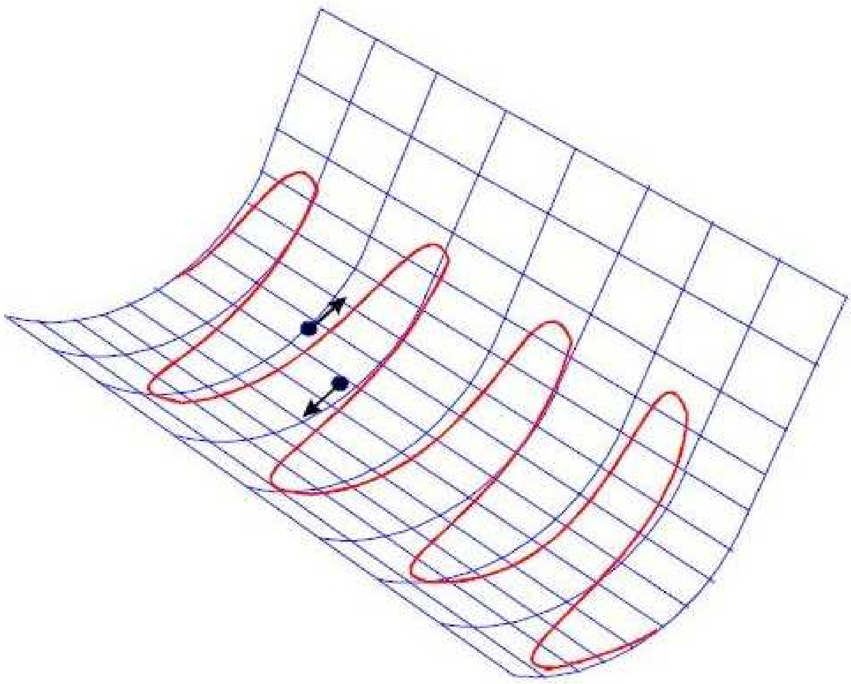

Figure 2.1: A view of a sphere rolling down a gutter as it is focused by the walls

The simplest cell pattern of a synchrotron lattice is the FODO (see chapter 1). Passing through this pattern of focusing and defocusing lenses, particles make oscillations. We can simply describe this motion thinking of small spheres (our particles) which roll down a slightly inclined gutter at a constant speed (see figure 2.1). These transverse oscillations are called **Betatron oscillations** and they exist in both horizontal and vertical planes. The number of such oscillations per turn is called **Tune** and is indicated with Q_x or Q_y (horizontal and vertical **tune** respectively)[1]. In our gutter example, the sphere makes four complete oscillations along the gutter: therefore $Q = 4$.

The tune value cannot be arbitrary chosen. Indeed at certain values of tunes, the oscillations tend to amplify and grow. At a resonance, the beam may be lost. To avoid dangerous phenomena for the beam, like resonances, a tune diagram is often used as a tool to position the tunes away from intabilities regions[1]. For this reason it is necessary to measure precisely the tune value.

2.2 Tune measurement system of the LHC

2.2.1 Excitation, Pick-up, Acquisition Chain and Digital Processing

The ability to measure the tunes is important for many kinds of diagnostic. The tune value of a circular accelerator can be measured by observing the betatron oscillations of the beam on a position sensitive pick-up. In frequency domain the betatron signal is seen as sidebands on the revolution harmonics [1].

In the base band tune (BBQ) measurement system developed at CERN [6], we use diodes to detect the envelope of the signal [7]. The signal is digitalized with a 24bit audio codec an is processed in the FPGA of the DAB (see chapter 1).

The acquired data (for the horizontal and the vertical plane) is filtered and decimated if oversampled to improve its resolution, windowed to reduce the spectral leakage and FFT trasformed. In order to perform a single FFT, the H (horizonatal) and V (vertical) plane data are mixed into a single complex signal (see figure 2.2). Two buffers are used to store the raw data and the FFT results [8].

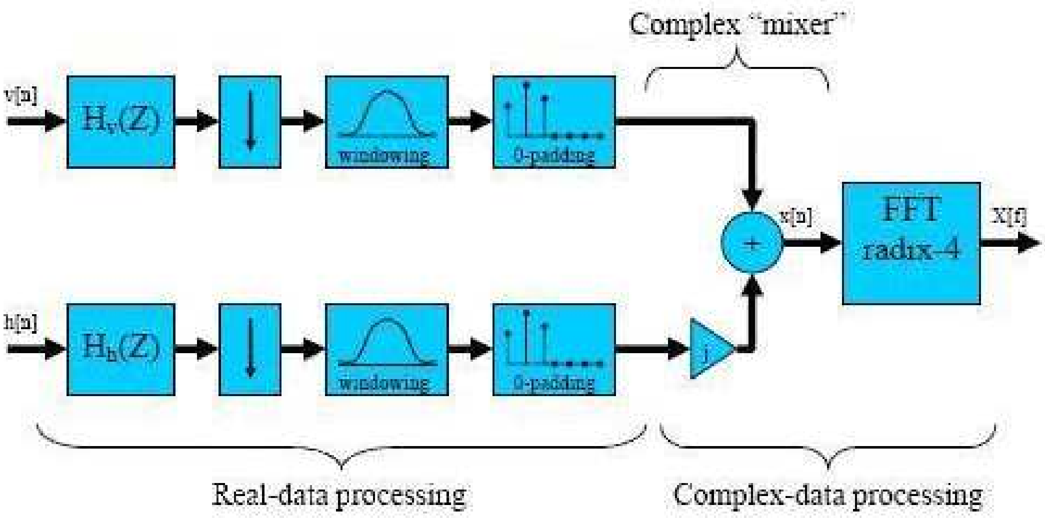

Figure 2.2: Digital processing chain for the Q measurements

Inside the FPGA two digital frequency synthesizers (DFS) were implemented to generate stimuli for the kickers. They can produce two different stimuli:

- a kick, which can excite all the frequencies
- a chirp, a signal in which the frequency increases ("up-chirp") or decreases ("down-chirp") with time. It can stimulate only some frequencies. Frequencies and amplitudes of chirp stimuli are programmable.

The acquisition and excitation triggers are internally generated to allow a full synchronization.

LabView (National Instruments) and a USB to VME bridge (CAEN VX1718) were used to test the FPGA code.

2.2.2 Setup for the tune measurement system of the LHC

Tune measurements setup is based on the CERB/BI standard acquisition system (see chapter 1) in which the power pc is substitued by the CAEN VX1718 module and a PC (see figure 2.3). The VX17 18 is a VME master module which can be

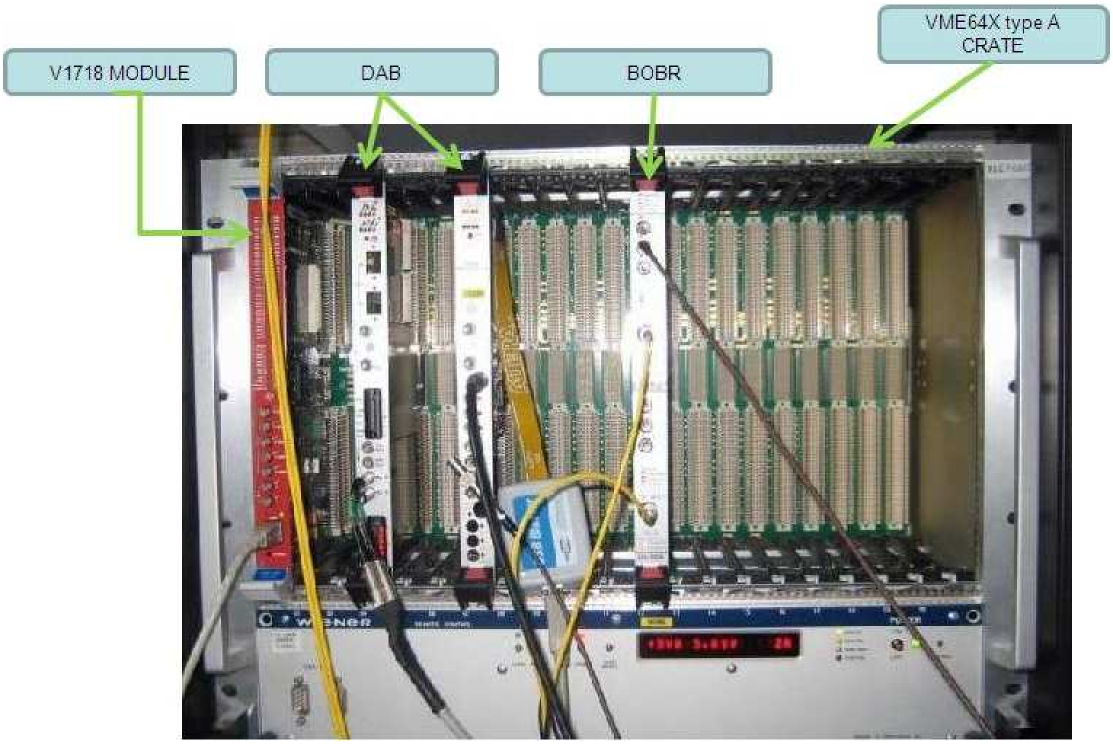

Figure 2.3: Setup for the tune measurement system of the LHC

operated from the USB port of a standard PC. It provides all of the addressing and data transfer modes documented in the VME64 specification.

This solution was adopted in order to have the possibility of using NI LabVIEW, appreciated for its simple graphic programming interface.

The DAB is equipped with a mezzanine board to provide the interface with the two DFS.

2.2.3 Post Mortem Data

In pathological conditions the beam can be lost in few turns. In order to understand more about a beam loss, it is useful to analyze the last received data before the ”beam death”. The DAB is equipped with a 512 kB - post mortem memory: this is responsible for the post mortem data storage turn by turn and is implemented like a circular buffer (see figure 2.4).

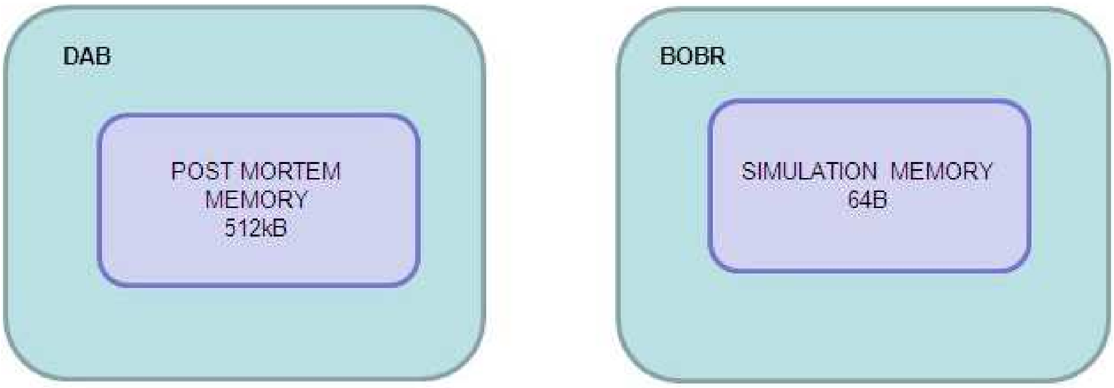

Figure 2.4: Post mortem memory and Simulation memory

I developed a software in LabVIEW to test this post mortem memory. The setup for this post mortem test is the same described in chapter 2.2.2 but in this case, instead of using the codec and the DFS, it is sufficient to use BOBR and DAB in simulating mode in order to simulate events of beam loss.

The BOBR can work in simulating mode, referred to as *Internal Mode*. The BOBR is also equipped with a simulation memory (SIM memory). This 64B-memory is used to send post mortem Start and Freeze (PM Start and PM Freeze, respectively) commands to the DAB. These two commands start and end the post mortem procedure, respectively. Also the DAB can work in simulation mode, referred to as *Loop back Mode*.

In figure 2.5 you can see the flow chart of my program developed to test the PM memory. In the *initialization* stage, I initialize the CAEN VME UBS Bridge Module, using the function *CAENVME Init*, implemented in the CAEN-VMELib. This function generates an handle to identify a module attached to the PC. I also set the simulating mode for BOBR and DAB.

After this initialization stage, the program sends a *PM Freeze* command and resets again the SIM ad the PM memories: I followed this procedure in order to remove any pending actions.

At this point I effectively started the testing procedure. The program sends a *PM Start command*, waits for a number of milliseconds equal to *MsecNum* and sends a *PM Freeze* command. Finally the program shows the raw data for both channels (see figure 2.7). While the program is waiting for the PM Freeze Com-

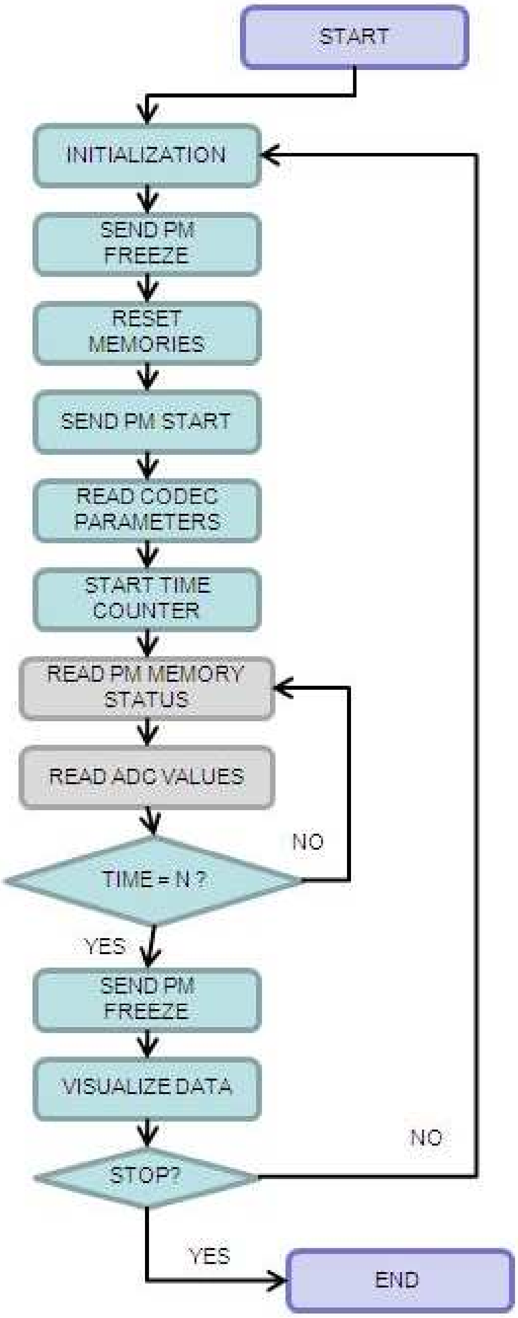

Figure 2.5: Flow chart of the program developed to test the PM memory

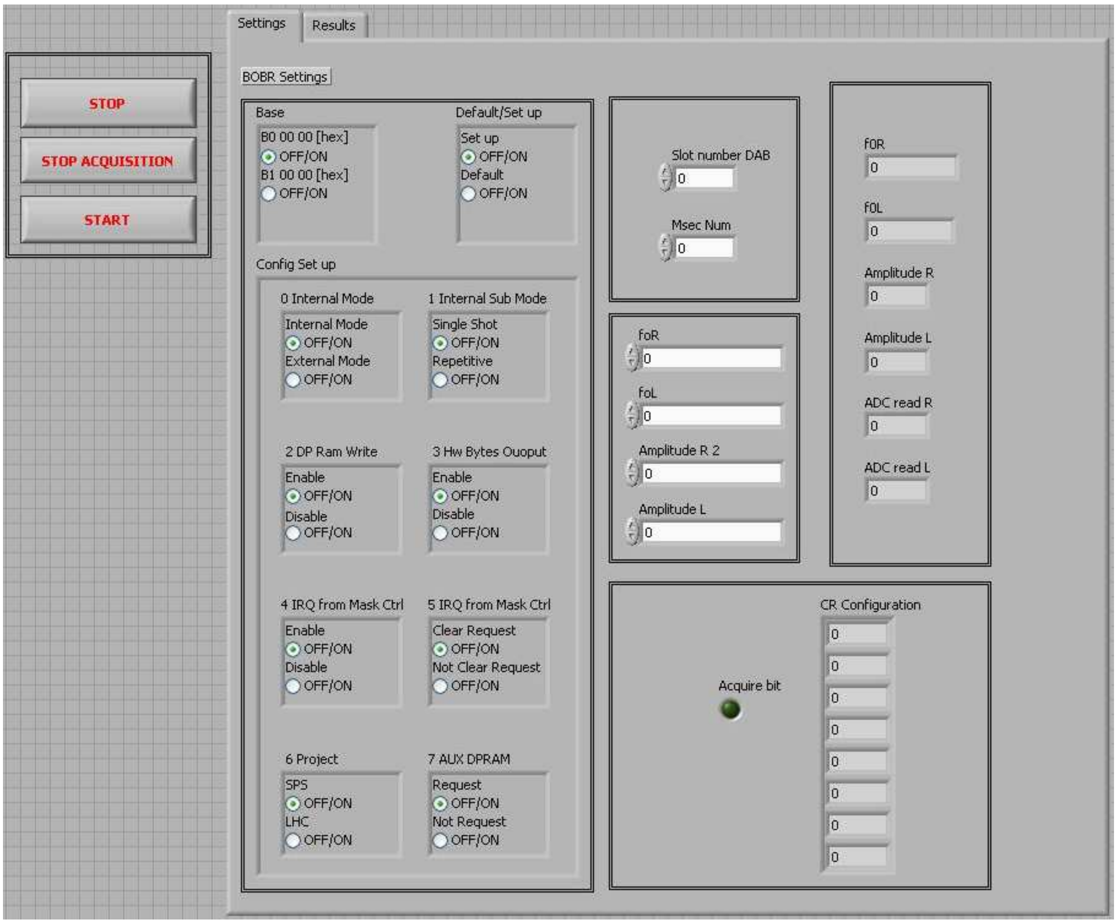

Figure 2.6: PM tool: Settings Tab Control.

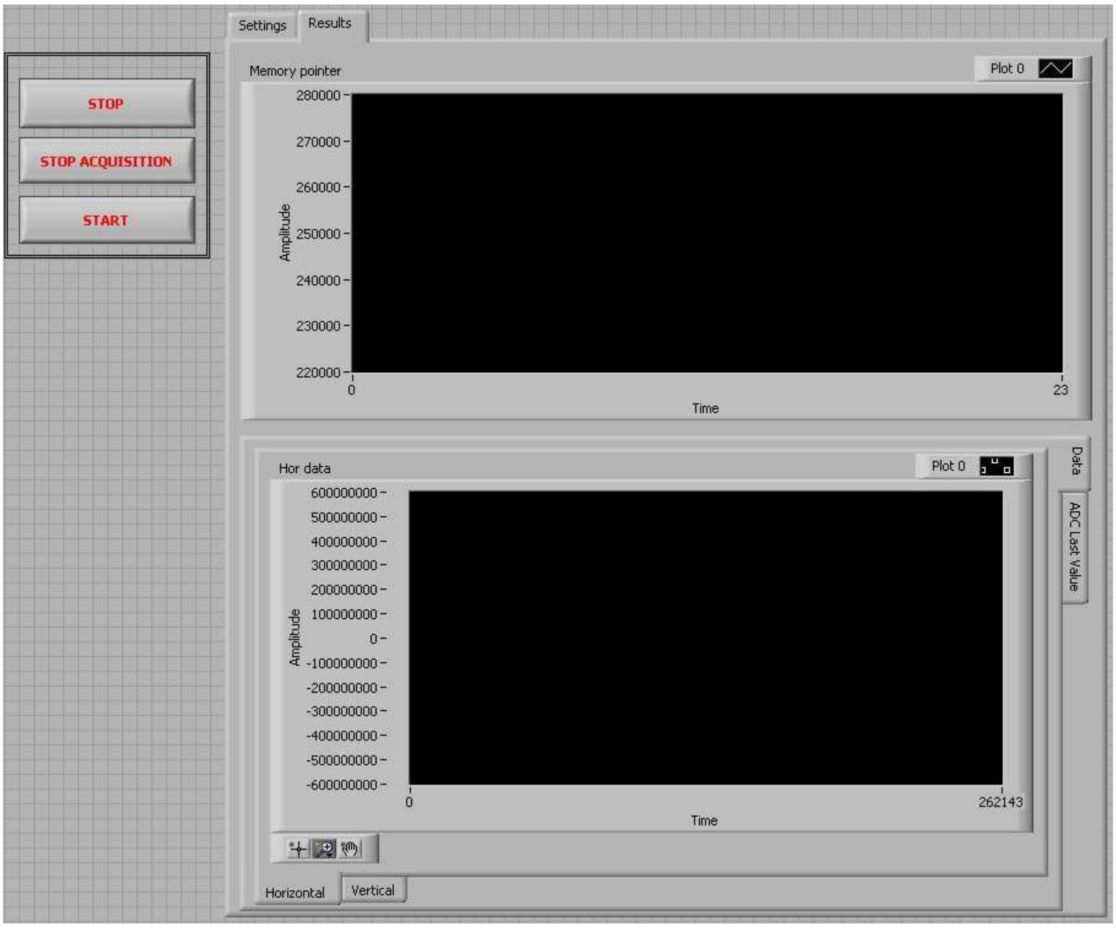

Figure 2.7: PM tool: Results Tab Control.

mand, it shows

- the status of the PM memory (memory pointer and acquisition bit)
- the last values read from the ADCs

I tested the PM memory with my software and the memory resulted fully working.

Chapter 3

Abort Gap Monitoring

3.1 What is the Abort Gap and What is it used for

The LHC is characterized by a very high energy stored on its beams (up to 350 MJ/ beam). The magnets in LHC can easily be damaged by even a very small fraction of the beam. In case of emergency, the beam is extracted from the rings using kicker magnets and is sent to a dump line which can absorbe a high energy.

In order to have this system working efficiently, we must leave a gap in the ring fill pattern with a length equal to the rise time of the abort kickers magnets: this gap is referred to as the **Abort Gap** and its lenght is 3.3 μs.

It is really important to assure that no particles accumulate in the gap since those would receive only a weak kick when the dump system is activated, and would hit machine components. The maximum charge density admissible in the gap can be calculated taking into account the machine energy and the damage threshold of the most sensitive components. The abort gap needs then to be monitored continously in order to dump the beam or activate gap clearing procedures in the event the safey threshold is reached.

CERN specifications [9] require an abort gap monitor to be able to detect a charge density of 60 p/ps with a spacial resolution of 100 ns long portion of the abort gap at 7 TV, with a 50% accurancy.

3.2 Principle of the Abort Gap monitoring system

There are different techniques to detect the presence of charged particles in the abort gap of the LHC: one of them is to observe the synchrotron light emitted by them.

3.2.1 The Synchrotron Radiation

Synchrotron radiation is the name given to the radiation which occurs when charged particles are accelerated in a curved path or orbit.

The loss energy per turn can be expressed as

$$\Delta E = \frac{k}{\rho} \left(\frac{E}{m_0} \right)^4 \tag{3.1}$$

where E is the energy of the particle, m_0 is the rest mass of the particle and ρ is the radius of curvature of the bending magnets. This means that the loss energy per turn scales as the fourth power of the particle energy. The synchrotron radiation clearly depends on the mass of the accelerating particle: the mass of the electron is roughly 2000 times smaller than that of the proton and, therefore, the loss energy rate per turn for the electron is over 10^{13} times the loss for a proton of the same energy in the same synchrotron. Moreover the inverse dependence of synchrotron radiation loss on radius argues for building the accelerator as large as possible.

3.2.2 The Acquisition Chain for the Abort Gap

The components of the acquisition chain of the abort gap (figure 3.1) are located at different levels: the surface, the underground area and the US45 zone, an intermediate area between them.

The synchrotron light extraction system extracts the LHC synchrotron radiation. This light signal is converted into a voltage signal by a Michrochannel Plate Photomultiplier (MCP-PMT, described in chapter 3.3.1). This device needs a gate signal to be activated: this signal, generated by the DAB (see chap-

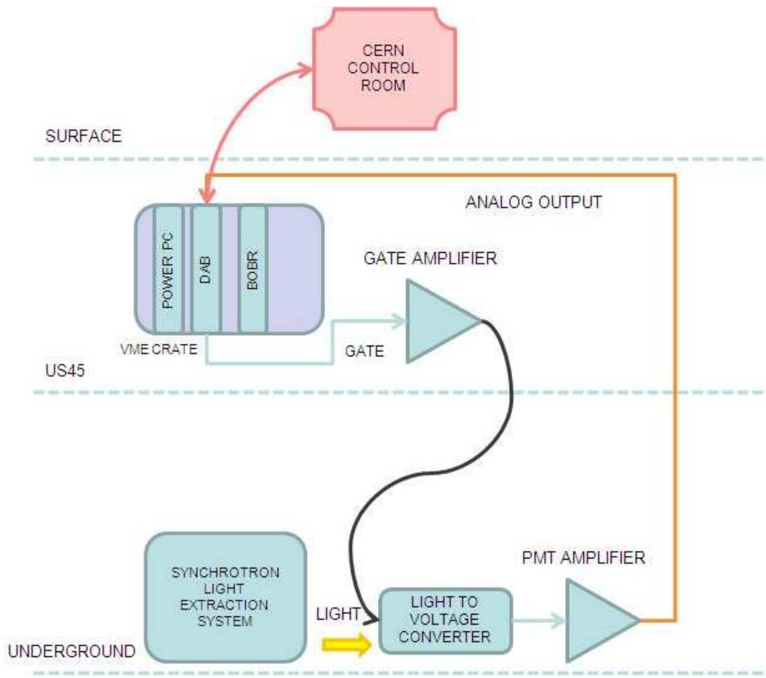

Figure 3.1: Physical position of the setup elements

ter 3.3.3), has to be carried from the US45 to the PMT and its amplitude has to be between 10 V and 50 V to activate the PMT. In order to assure that, we introduce an amplifier between the DAB and the PMT, called the *gate amplifier*. The 100 m long coaxial cable used to carry the amplified gate signal to the PMT is a DRAKA COMTEQ CB50. The voltage signal generated by the PMT has to be carried until the US45 zone (over 100 m of cable): therefore we introduce here an amplifier, referred to as *PMT amplifier*. This is an High Speed Amplifier C5594 Series, HAMAMASTU; it is designed as the most suitable amplifier unit for photomultiplier tubes. This unit has a high gain of 36 dB (voltage amplification of 63) and wide frequency bandwidth of 50 Hz to 1.5 GHz, which can accurately amplify the PMT pulse output. The cable used to carry the signal generated by the PMT to the US45 zone is a CK50 coaxial cable. The DAB is plugged in a VME crate with the BOBR and this system, controlled by a power pc is the standard BI solution for the data acquisition (see chapter 1). Finally the output signal coming from the DAB is carried to the surface, to the CERN Control Room.

3.2.3 LHC synchrotron radiation extraction system

The synchrotron radiation produced for the LHC depends on the working energy of the machine. For low energies, such as the ones used at the injection moment in LHC (which corresponds with the maximum energy of SPS) the ability to generate synchrotron radiation by bending magnets is limited. For this reason to increase the radiation at low energy it is necessary to add a *undulator* in LHC to allow the study of the beam at low energy using synchrotron radiation. The undulator only contributes significantly up to $1\ \mathrm{TeV}$, when the contribution of the bending magnets becomes predominant.

Figure 3.2: Undulator

In LHC there is a synchrotron light extraction system called **telescope**. It is made up of different optical elements. The synchrotron light is converted into a voltage signal and carried on the surface.

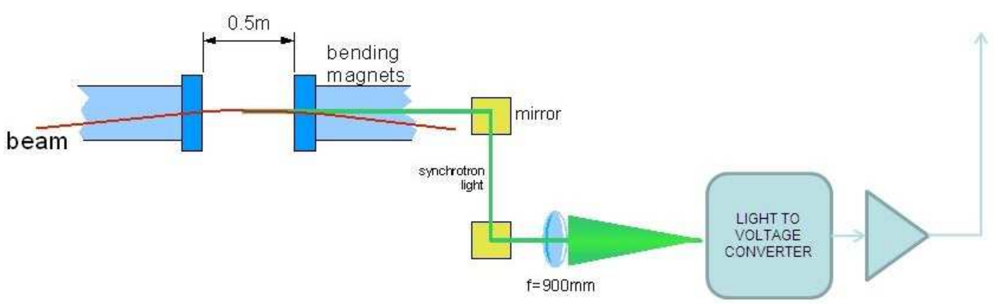

Figure 3.3: Telescope

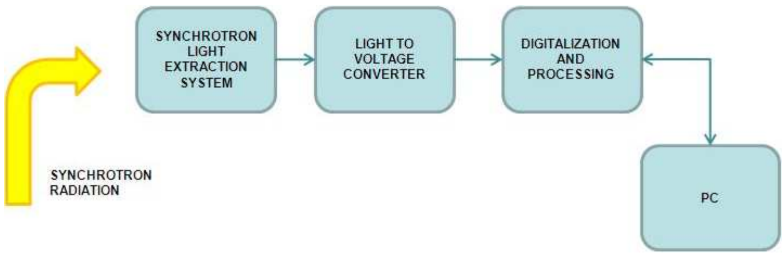

Figure 3.4: Conceptual Diagram of the CERN/BI solution for the abort gap monitorer

3.3 CERN/BI solution for the Abort Gap Monitorer

In figure 3.4 I show a conceptual diagram of the CERN/BI solution for the abort gap monitorer: the synchrotron light coming from the LHC is converted to a voltage signal which is digitalized and processed in order to extract the existent light intensity level.

3.3.1 The light - to - voltage converter

In order to satisfy CERN specification (see chapter 3.1), a MCP-PMT (Michro Channel Plate Photomultiplier) is chosen like device to convert the synchrotron light into a voltage signal.

A photomultiplier tube is a vacuum tube consisting of an input window, a **photocathode**, **focusing electrodes**, an **electron multiplier** and an **anode** usually sealed into an evacuated glass tube.

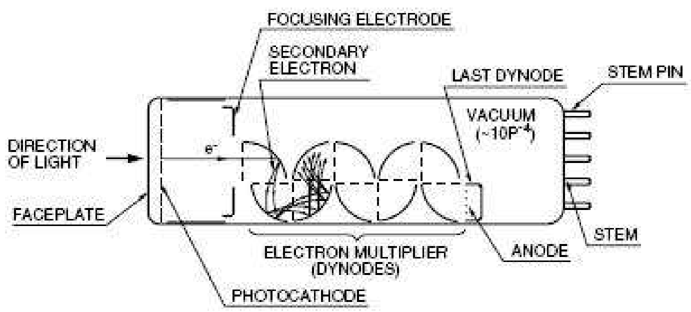

Figure 3.5: Sketch of a photomultiplier tube.

Figure 3.5 shows the schematic construction of a photomultiplier tube. Light which enters a photomultiplier tube is detected and produces an output signal throught the following processes:

- Light passes throught the input window.
- Visible photons hit the photocathode so that photoelectrons are emitted into the vacuum.
- Photoelectrons are accelerated and focused by the focusing electrode onto the first dynode (one of a series of elecrodes within a PMT) where they are multiplied by means of secondary electron emission. Each dynode is more positively charged than its predecessor. Secondary emission occours at the surface of each dynode.
- The multiplied secondary electrons emitted from the last dynode are finally collected by the anode.

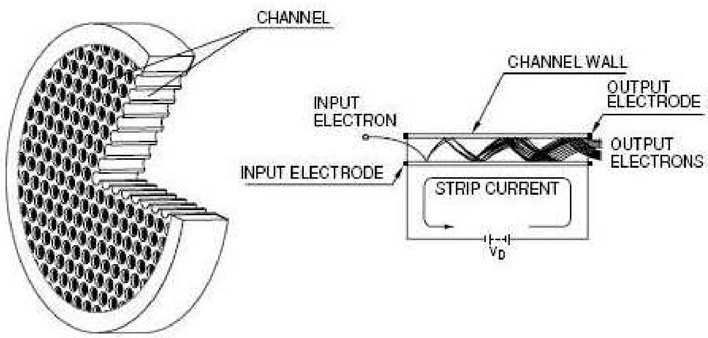

Figure 3.6: Schematic structure and principle of multiplication of a MCP.

Microchannel plates are compact electron multipliers of high gain. They are quite different from discrete dynodes and therefore offer high gain despite compact size, fast time response and low power consuption. Figure 3.6 illustrates the schematic structure of an MCP. The MCP consists of a two - dimesional array of a great number of glass capillaries (channels) bundled in parallel and formed into the shape of a thin disk. Each channel as an internal diameter raging from 6 to 20 μmwith the inner wall processed to have the proper electrical resistance and secondary emissive properties. Accordingly, each channel acts as an indipendent electron multiplier [12].

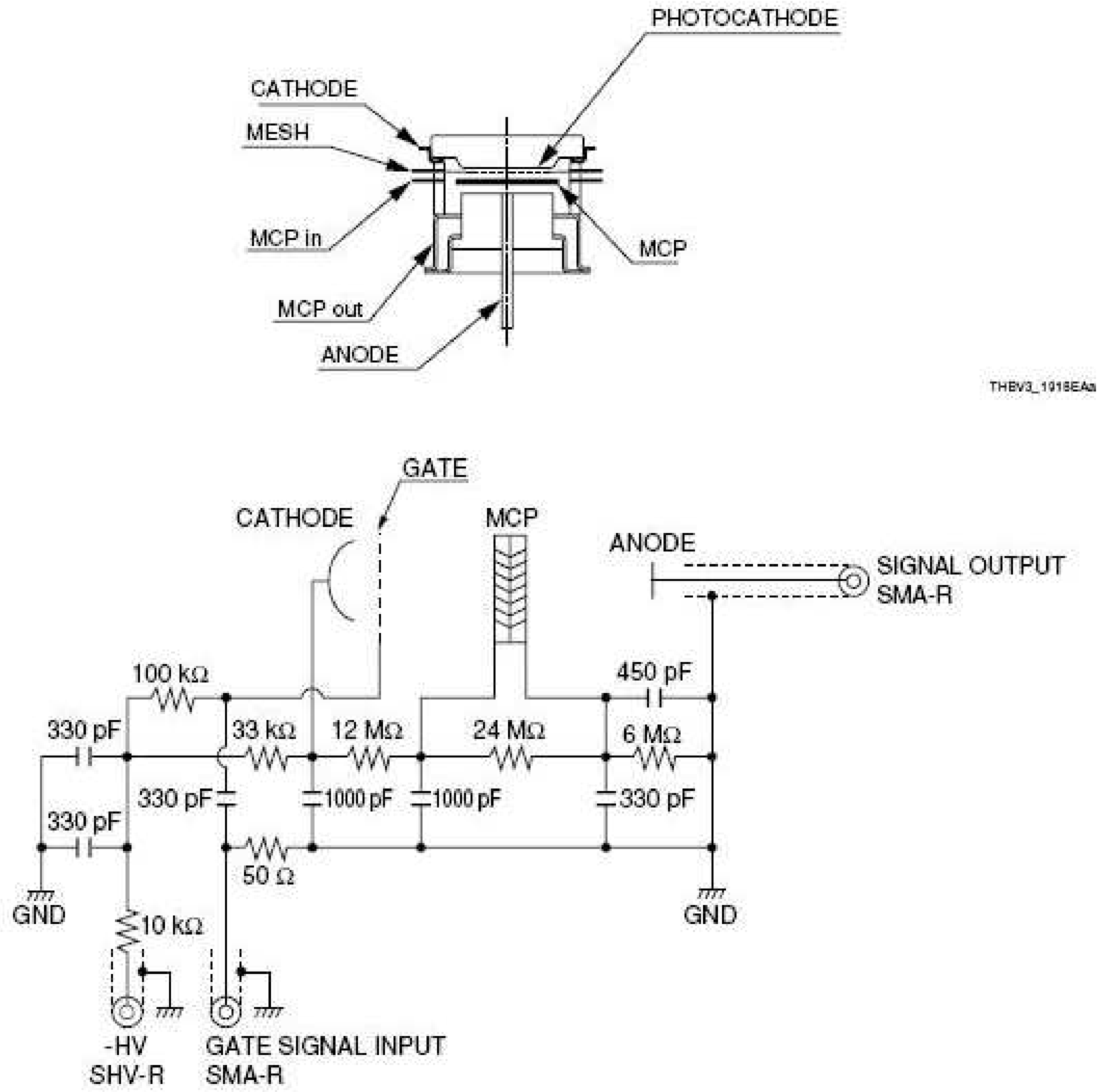

Figure 3.7: Structure of MCP-PMT R5916U50.

CERB/BI solution uses a MCP-PMT R5916U50: figure 3.7 illustrates its structure. This tube basically consists of a photocathode, **gate mesh**, MCP and anode. The gating function is performed by controlling the gate mesh which is positioned in close proximity to the photocathode as shown in figure 3.7. Applying a reverse potential with respect to the photocathode potential to the gate mesh sets the ’off’ mode, while applying a forward potential sets the gate operation ’on’ mode.

This MCP-PMT is chosen for:

- its high gain;
- its fast gate;
- its low noise;
- low voltage is required to gating it;
- its small dimension;
- it is commercially available.

3.3.2 Digitalization and Processing

In order to digitalize and process the signal coming from the light to voltage converter, CERN/BI solution uses the standard aquisition sytem (VME64X type A crate, DAB and BOBR) described in chapter 1 equipped with a dedicated mezzanine (IBMS mezzanine (see figure3.8)).

The IBMS mezzanine performs an analogical integration before digitalizing data (figure 3.9). This integration is performed by an ASIC developed for CERN in the *Laboratoire de Physique Corpusculaire of Clermont-Ferrand(France)*. This ASIC has 8 channels to enable a continuous parallel integration with a minimum period of 25 ns. Each channel has two integrators which are time-multiplexed to perform a continuous integration: while an integrator is integrating, the value of the other is made available. For the abort gap, the integration intervals are 100 ns, as required by CERN specification. Some tests show that these two integrators are not fully linear and there are differences their gains and offsets. Because of these differences, the integrators saturation points are different and we have artificial variations of the measured data: for this reasons it is necessary to equalize their gains and offsets. I developed a software to calibrate them, described in chapter 5. I also effectively calibrated them for a particulare mezzanine (indicated with number 419): results are also described in chapter 5.

Figure 3.8: IBMS Mezzanine

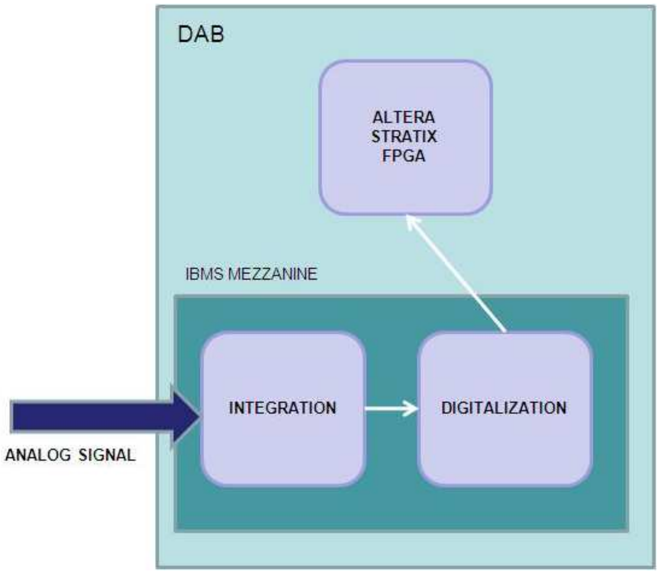

Figure 3.9: Conceptual diagram of the data digitalization and processing block

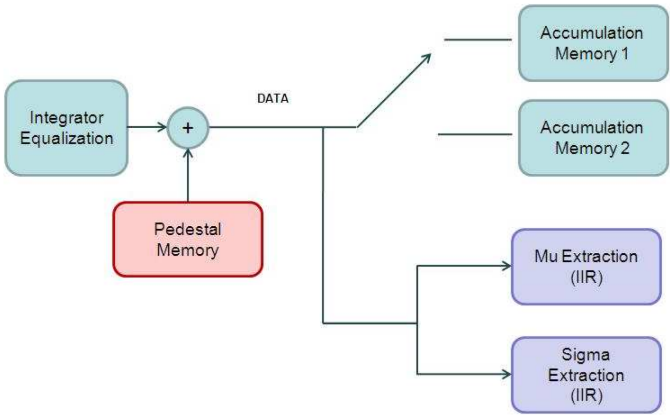

Figure 3.10: Digitalized Data Processing chain

After the integration, the signal is digitalized with a 14-bit ADC and it is made available on the output mezzanine pins.

The digitalized signal is analyzed by the Stratix FPGA (integrated in the DAB) which is the "smart" section of the data treatment system for the abort gap. The data coming from the mezzanine are multiplied by a gain factor and added to an offset value in order to equalize the integrators parameters. Acquired data can be affected by systematic errors: in order to correct them, a Pedestal memory was introduced : a pedestal value is subtracted from each reading (see figure 3.10). The LHC abort gap monitorer has to perform a continuous acquisition analyzing 100ns long portions of the abort gap; it is also required to estimate the average of the measured data and the error of this estimation. In order to satisfy them, the FPGA module generates an aquisition window divided in 64 bins ($100\ \mathrm{ns}$). Using this window, at each turn we acquire data and we accumulate them in a memory buffer called *Accumulation Memory*. We can choose the number of turns of this accumulation between 1 and 262144 (about $23\ \mathrm{second}$): I refer to this value as *observation period*. At the end of the obsevation period an interrupt is sent on the VME bus to inform that new data is available in the buffer. During the acquisition we use alternatively two buffers (Accumulation memories 1 and 2) in order to avoid dead times.

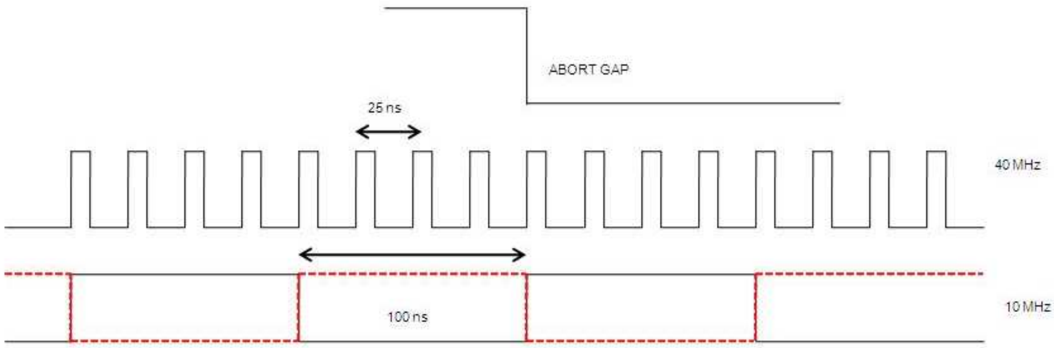

Figure 3.11: Turn clock and sampling clock

The FPGA implements also an IIR lowpass filter, which is an improvement with respect to the basic requirements:

$$y[n] = (1-a)\,y[n-1] + ax[n] \tag{3.2}$$

where the coefficient a is programmable. We use this filter to average the acquired data and calculate also the second order statistics value: these results are stored in two memories, called respectively *Mu* and *Sigma* memories.

As described in chapter 2, BOBR provides a 40MHz clock. We sample the analog signal every 100 ns. We can obtain this 10MHz sampling clock by the turn (40MHz) clock, but in this way we can have a phase uncertainty of this clock with respect to the turn period (see figure 3.11). In order to avoid this uncertainty, the sampling clock is resynchronized with respect to the turn clock. The phase relation between them can be set in steps of 12.5 ns.

3.3.3 The MCP-PMT control

The MCP-PMT needs a gate signal to be activated: this signal is generated by the Startix FPGA integrated in the DAB (see chapter 3.2.2).

The FPGA can generate a gate with programmable length. In order to synchronize the gate with the abort gap, it is possibile to move the gate position inside the revolution period with respect to the rising edge of the turn clock in

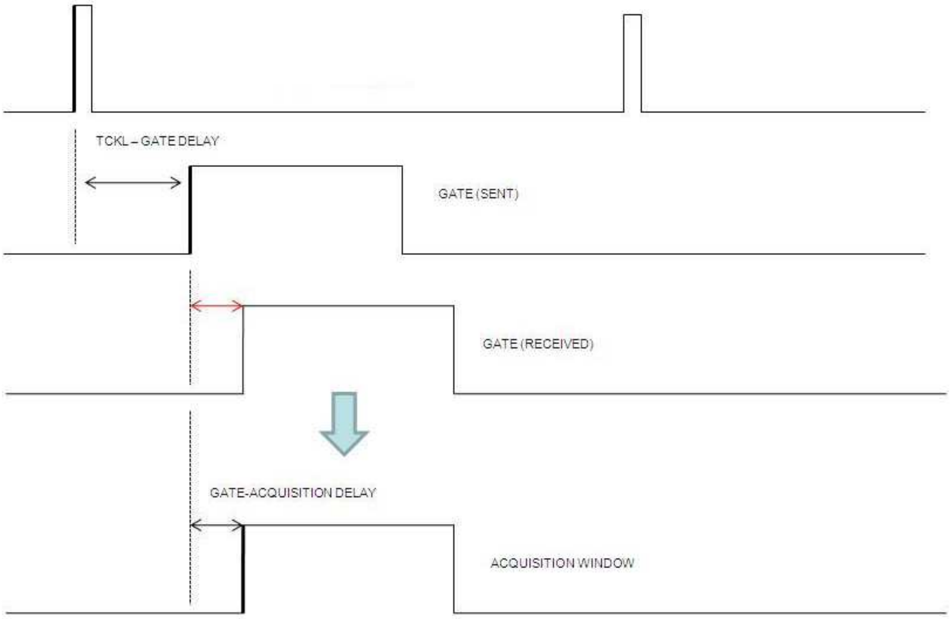

Figure 3.12: Turn clock, gate and acquisition window delays

steps of 25 ns.

Since the gate signal has to be sent from the DAB to the PMT and sent back again (see figure 3.1), it can be affected by delays. In order to compensate them, the FPGA can also adjust the start of the acquisition, moving the start of the acquisition window with respect to the gate start in steps of 25 ns.

Chapter 4

Data Treatment for the Abort Gap

4.1 Testing setup in the laboratory

One of the goals of my project was the setup system developing for the abort gap in order to verify the synchronization procedure with the FPGA and the performance of the acquisition chain (noise).

To reach my purposes, it was necessary to be able to generate powered-controlled light pulses, with programmable width and to be able to move their position inside the revolution period.

Because of that I generated light pulses with a photodiode (LED Blue-Green RS 228-1863) controlled by a pulse delay generator (Standford Research System DG535, see figure 4.2). This pulse delay generator was chosen because it gives the possibility to control separately the pulse width and the pulse delay with respect to an internal trigger. I used optic filters to perform an accurate adjustement of the intensity light emitted by the photodiode.

The light pulse emitted by the photodiode is the input signal for the MCP-PMT, which is activated by a gate signal coming from the DAB and amplified (see chapter 3). The output signal coming from the PMT is carried to the DAB to be digitalized and processed.

The DAB is plugged in a VME crate together with the BOBR: instead of controlling this system with a power pc (like in the BI standard solution for the data acquisition, see chapter 1), we use the CAEN VX1718 module and a standard

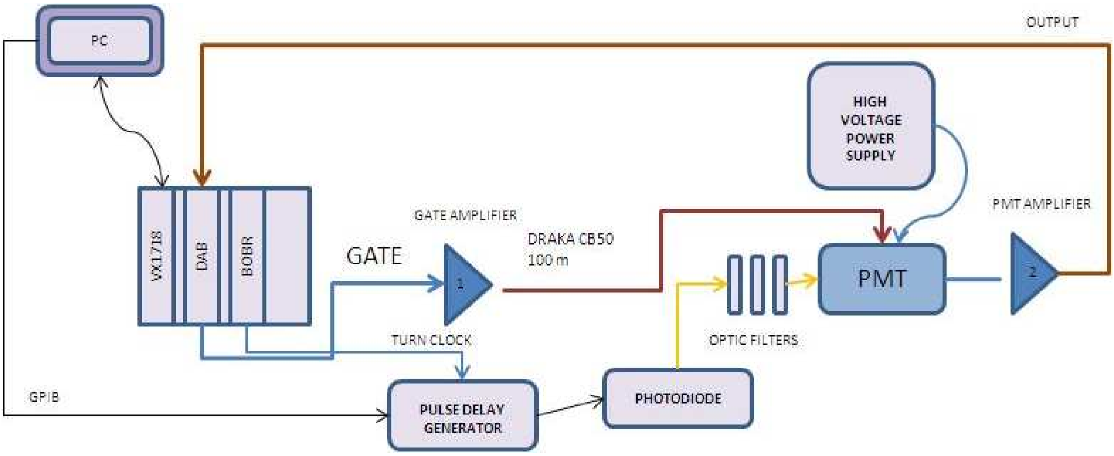

Figure 4.1: Testing Setup

PC, as done for the tune measurement (see chapter 2). The DAB is equipped with a IBMS mezzanine, as described in chapter 3. My software tool allows to control and to interface with the Stratix FPGA, integrated on the DAB.

Figure 4.2: Pulse Delay Generator

I used a HEIDEN Quint DC power supply 1129 (see figure 4.1) to power the gate amplifier (±15 V) and the PMT amplifier (±12 V). I used a FUG High Voltage Power Supply HCN 140-3500 to power the PMT (see figure 4.1). To display and check our signals I used the oscilloscope Le Croy waverunner, 6000A series (figure 4.5).

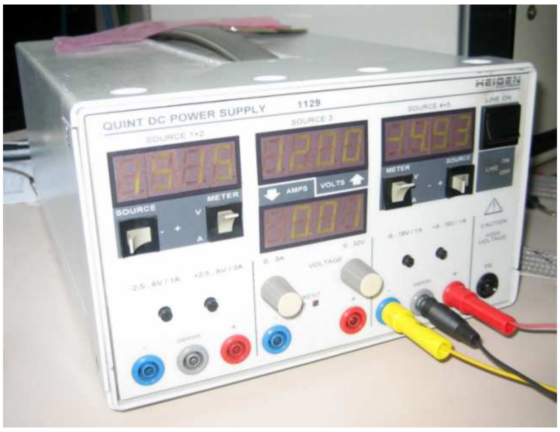

Figure 4.3: HEIDEN Quint DC power supply 1129

Figure 4.4: FUG High Voltage Power Supply HCN 140-3500

Figure 4.5: Oscilloscope

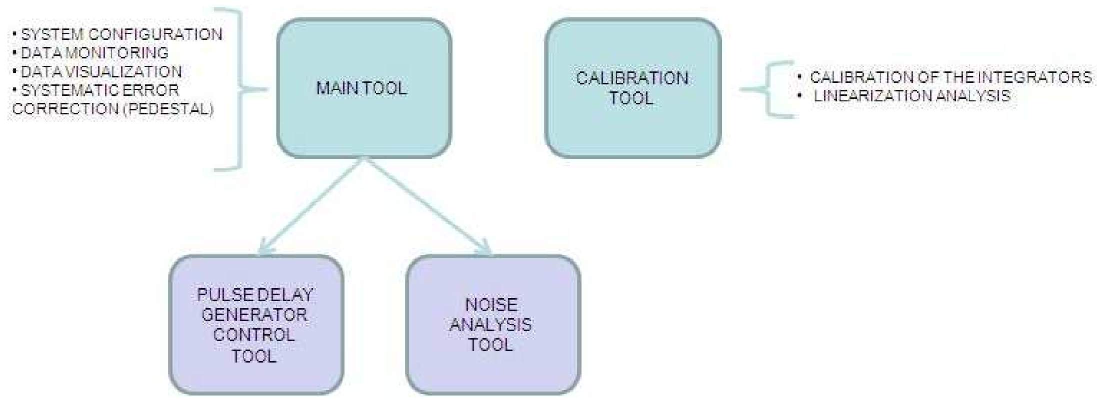

Figure 4.6: Software Tools Overview

4.2 Software tools for the abort gap monitoring

The developed LabVIEW software package encompasses two principal tools (see figure 4.6): the *Main* tool and the *Calibration* tool. The Main Tool provides:

- the complete system configuration;
- the data monitoring;
- the data visualization;
- the systematic errors correction with the Pedestal memory.

Moreover, from the Main tool it is possible to call two important subVIs: the *Noise Analysis* tool which performs the noise analysis of the chain (see chapter 4.2.3) and the *Pulse Delay Generator control* tool which remotely control the pulse delay generator via GPIB. All the controls of this instrument can be set properly in order to perfom an automatic measurement of the output signal amplitude when we move its position inside the revolution period (see chapter 4.3.3). The *Calibration* tool performs the integrators equalization (see chapter 3) and the procedure (described in chapter 4.2.2.1) to linearize their characteristics. This software and the FPGA one were developed in parallel, in order to perform a progressive check of the implemented algorithms, of the results and of possible further solutions. *Calibration* and *Noise Analysis* tools can perform their analysis in an on-line modality: the collected measured values are stored in arrays and processed. However these tools can also analyze data stored in files: this functionality is useful when the measurements amount is huge or simply we are interested in performing our analysis in a different moment. I used this second modality especially to test different algorithms, without repeating the measurements.

4.2.1 The Main tool

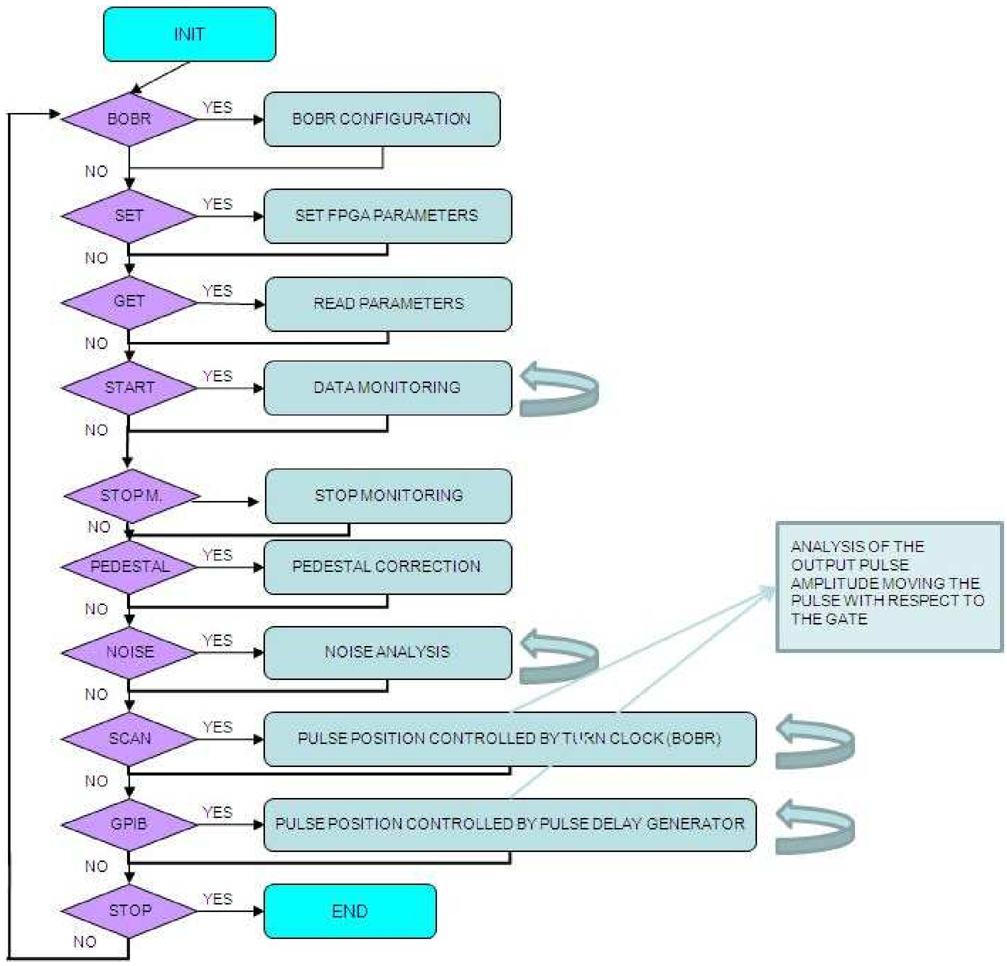

Figure 4.7: Flow chart of the main tool. Flow charts of the stressed tasks are shown in the following.

My program initializes the CAEN VME UBS Bridge Module using the function *CAENVME Init*, implemented in the CAENVMELib (see chapter 2). It also

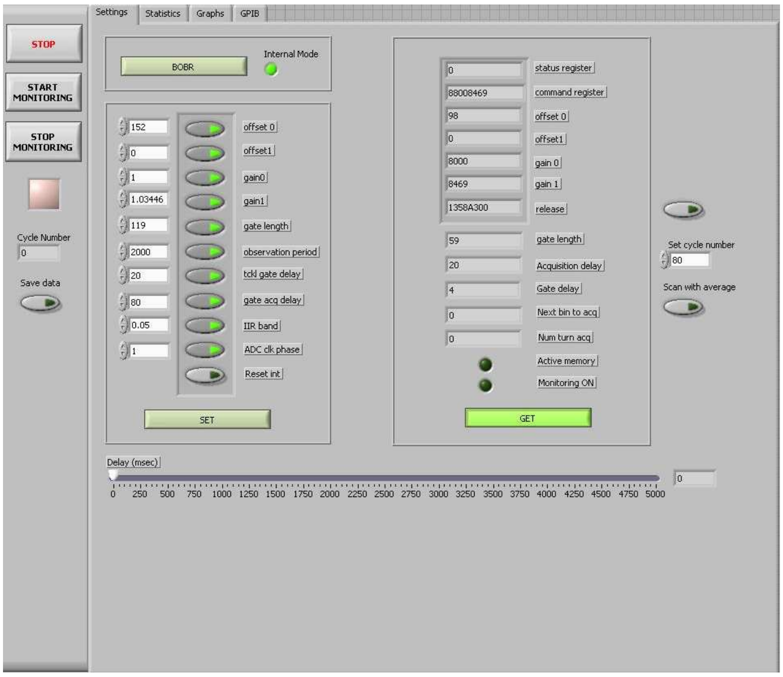

Figure 4.8: Main tool: Settings Tab Control.

initializes and clears the interrupts (see chapter 3) and sets the Pedestal memory locations to zero.

The program sets all the control parameters for the FPGA described in chapter 3 (see figure 4.8): integrator gains and offsets, observation period, gate length, gate position inside the revolution period (*Turn clock - Gate Delay*), aquisition window delay with respect to the gate (*Acquisition - Gate delay*), IIR filter coefficient and sampling clock delay with respect to the turn clock (*ADC clock phase delay*). The program can also read all the set parameters (*Get* command).

The task responsible for the data monitoring creates files and folders to store the acquired data, clear the interrupts and starts the monitoring (see figure 4.9). As described in chapter 3, when data are available in one of the two accumulation memories, I receive an interrupt with status equal to 1 or 2 (depends on the memory). The program is able to complete the reading of one of these two memories while the other is accumulating data. The monitoring task can be stopped manually or automatically.

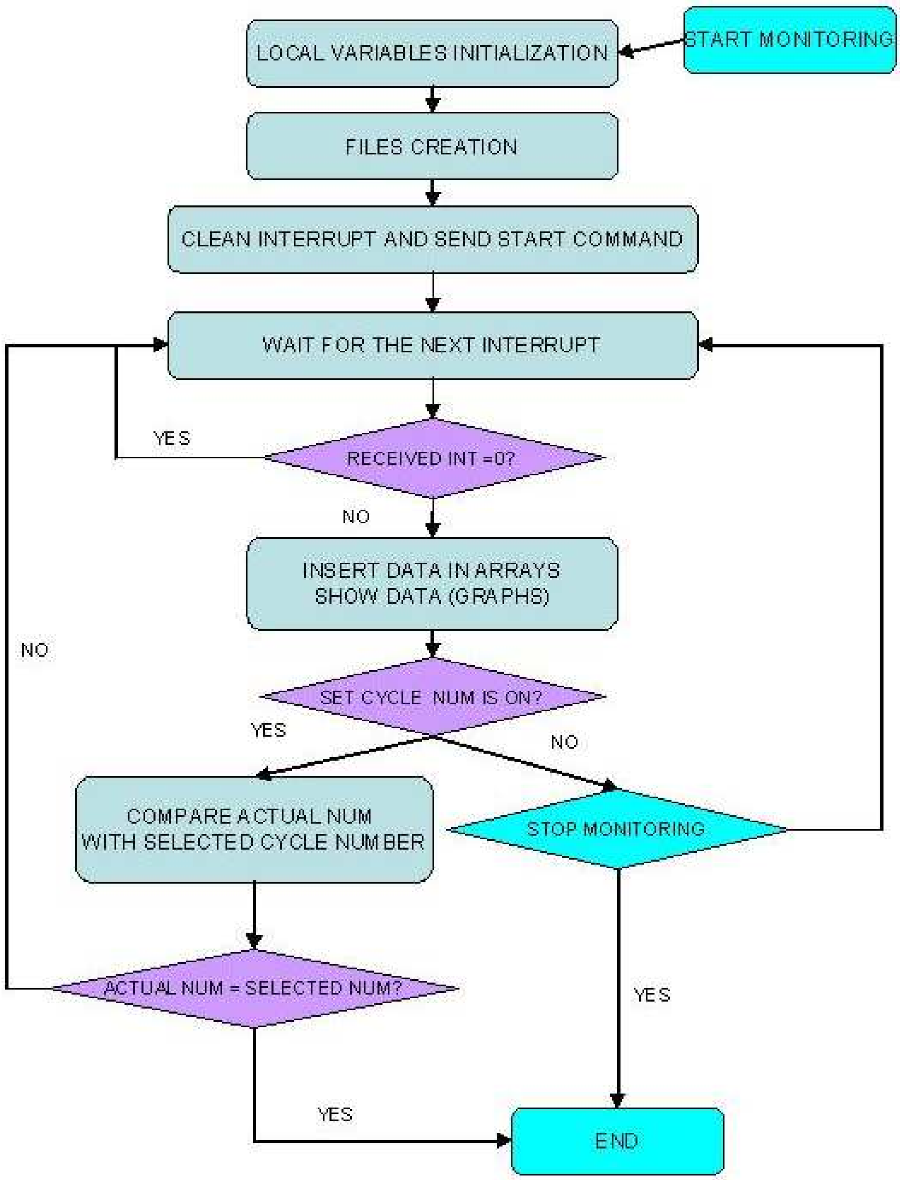

Figure 4.9: Flow Chart of the Start Monitoring vi.

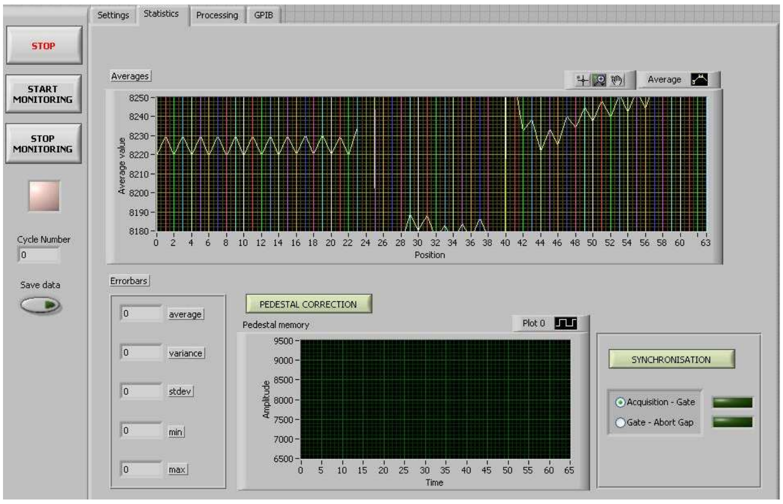

Figure 4.10: Main tool: Statistics Tab Control.

During the data monitoring, my program shows the data read from the *Accumulation memory* and the average of these data (read from the *Mu memory*) with the standard deviation values (read from the *Sigma memory*), represented by errobars (see figure 4.10).

When the signal monitoring finishes, my program sends a *Stop Monitoring* command to the FPGA, cleans the interrupts and saves data on files if the optione *Save* is set. Moreover graph are saved in the jpeg format.

The program can perform a data correction, using the *Pedestal memory* (see chapter 3) and an analysis of the noise in our system (described in chapter 4.2.3), using the *Noise Analysis* subVI.

The two tasks referred to as *Scan* and *GPIB* perform the analysis of the amplitude of system output signal when I move its position with respect to the gate (this analysis is described in chapter 4.3.3).

With the *Scan* task, I can control the photodiode using a 25 ns long pulse, generated by the BOBR and change the gate position inside the revolution period (*Tclk - gate Delay*, see figure 4.11). I performed this procedure because initially I could not use the pulse delay generator to change the pulse position with respect to the gate signal.

With the *GPIB* task (see figure 4.13), instead, I can perform a remote control of the pulse delay generator and change the pulse position with respect to the

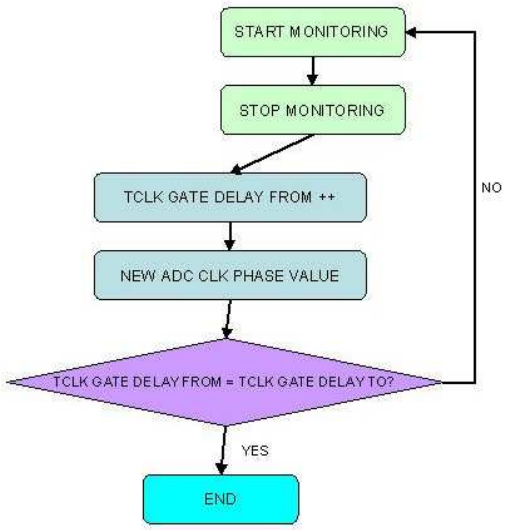

Figure 4.11: Flow Chart of the Scan vi.

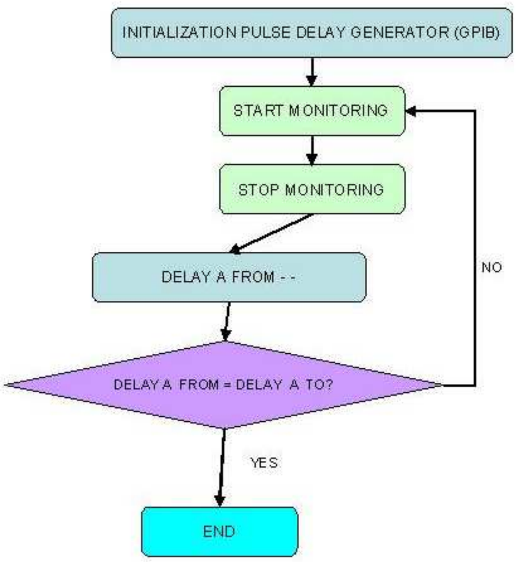

Figure 4.12: Flow Chart of the GPIB vi.

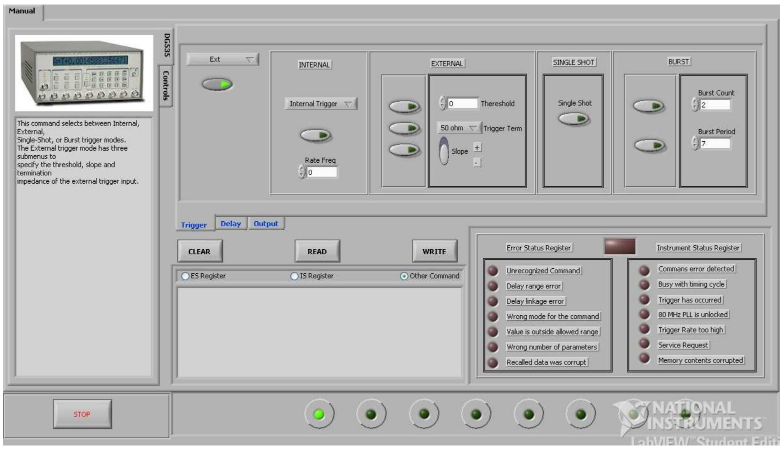

Figure 4.13: User Interface to remotely control the pulse delay generator.

gate signal. In order to do that, at each start of the data monitoring, I change properly the A channel delay of the pulse delay generator (see figure 4.12).

To analyze the changes amplitude of the output signal, the second described approach was preferred for two reasons:

- currently, we want to test the real system moving the pulse with respect to the gate signal and not the opposite;
- if we generate the pulse by means of the BOBR, we can't change its width.

My results of this analysis, described in chapter 4.3.3, were obtained using the *GPIB* task.

4.2.2 Mezzanine Calibration

4.2.2.1 The Calibration Procedure

As described in chapter 3, the goal of this mezzanine calibration is to equalize gain and offset of one of the two mezzanine integrators with respect to gain and offset of the other one (which we do not affect - its gain and its offset equal to 1 and 0 respectively). In order to perform that, I follow this procedure:

- determining the two integrators characteristics;
- making a linear fitting of these two curves;

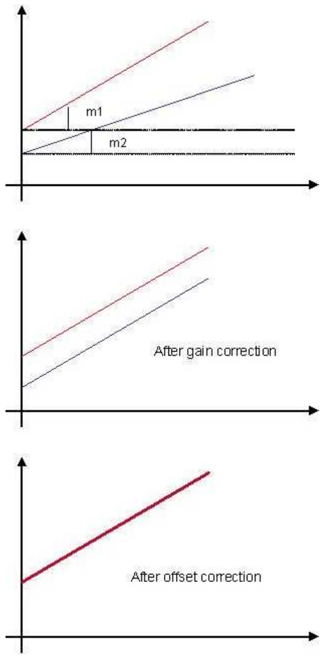

Figure 4.14: The Calibration Procedure

- calculating the gain as the ratio of the two characteristics slopes;
- determining the offset as the difference of the two characteristics.

As expected, the integrators charactersitics are not fully linear. I investigated whether linearizing them was possible; alternatively, a piecewise linearization had to been performed. I progressively increased the input voltage to understand how much the characteristics linearization was degraded by this voltage increasing.

I measured the output values in correspondance of input voltage between $-32\ \mathrm{mV}$ to $32\ \mathrm{mV}$ with a step of $1\ \mathrm{mV}$: I considered progressively increasing ranges of these measure samples (referred as to *Sample Ranges*) and I applied the described procedure to calculate gain and offset for each one. I corrected the integrators characteristics with each gain - offset pair and I calculated the relative square errors (SEs) between them: finally, I analyzed the error trends in correspondance of the input voltage range.

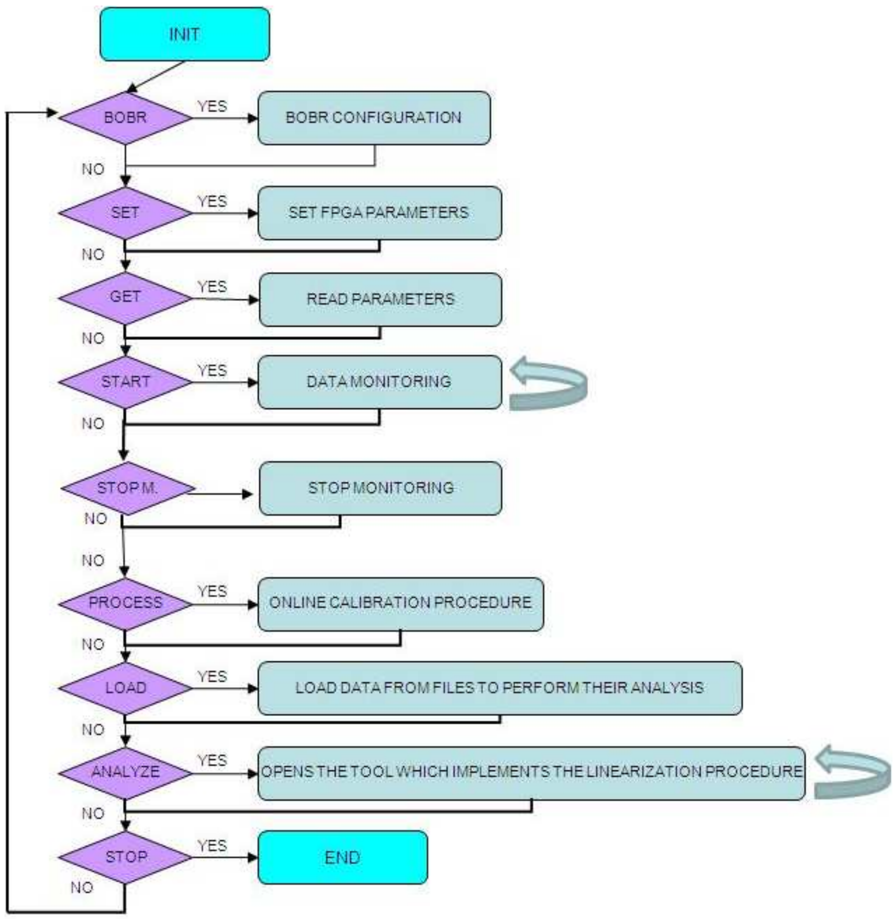

Figure 4.15: Flow Chart of the calibration tool

4.2.2.2 The Calibration Tool

The goal of my tool is to perform the described calibration procedure. This program encompasses some tasks mentioned in the Main Tool (see figure 4.15)as the system initialization and the data monitoring.

My program can estimate gain and offset and show the integrators characteristics with an online procedure (referred to as *Processing*), as shown in figure 4.16. It can also perform a more sophisticated calibration, in order to study the relationship between gain and offset values and the input voltage range (see figure 4.17).

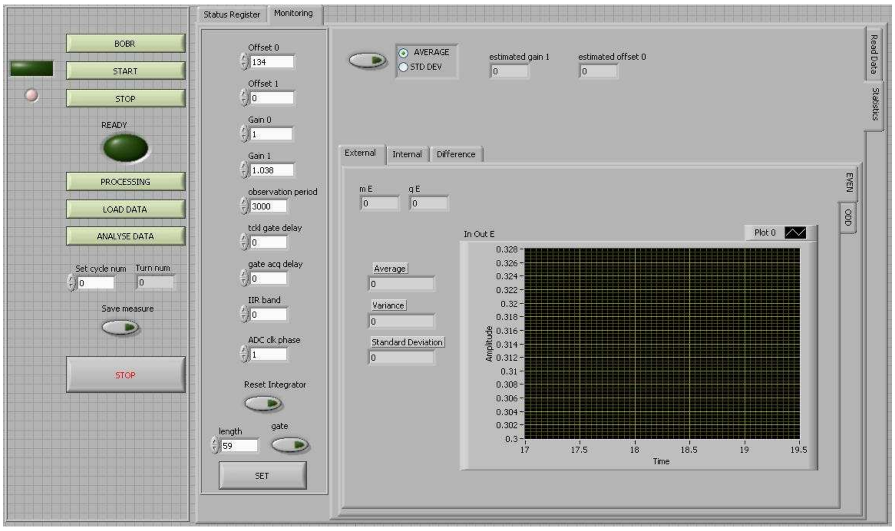

Figure 4.16: Tool fot he calibration: Monitoring- Statistics Tab Control

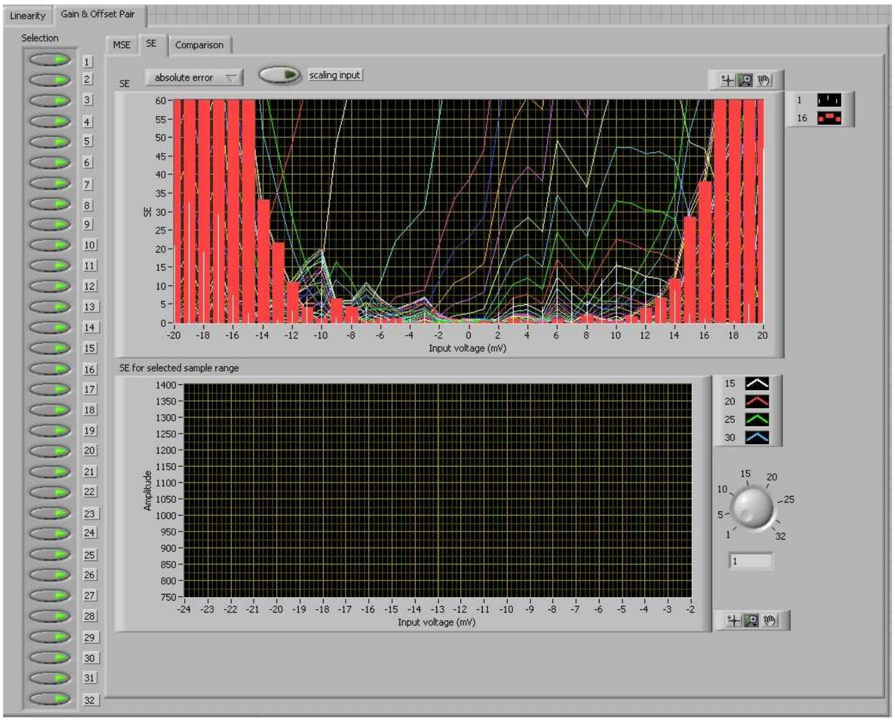

Figure 4.17: Tool for the calibration analysis: Tab control Gain and Offset- SE

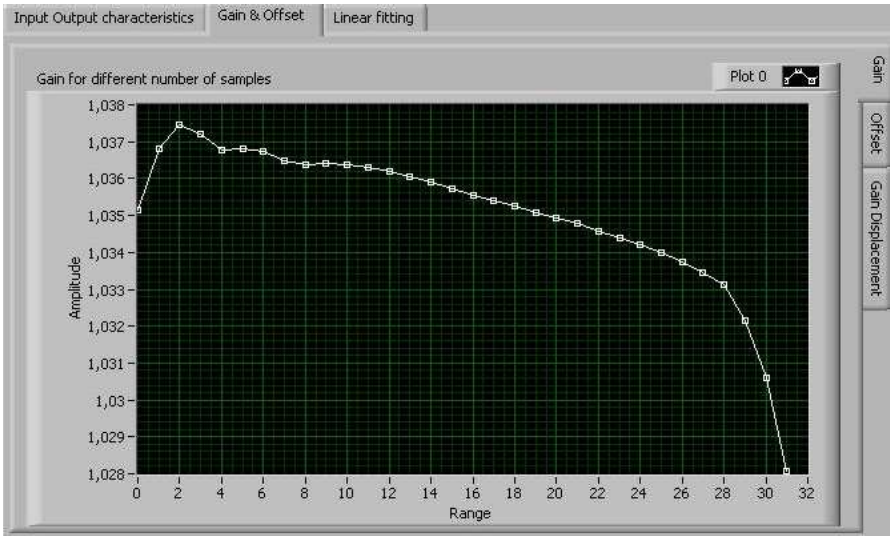

Figure 4.18: Tool for the calibration analysis: Tab control Gain and Offset

My program gives the square error curves and the gain and offset trends for each *Sample range* (figure4.18).

With my software I calibrated the mezzanine 419 as described in chapter 4.3.1.

4.2.3 The noise analysis

4.2.3.1 The noise analysis procedure

The goal of the noise analysis is to estimate the performance of the system, to determine the most noisy component of our chain and to compare the measured noise with CERN requirements.

I can divide the testing setup chain in three blocks (see figure 4.19):

- the first block corresponds to the DAB and to all its electronic components. I referred to the noise level after this section as N_{ID}.
- the second block encompasses the gate amplifier, the CB50 coaxial cable and the PMT. I referred to the noise level after this section as N_{PMT}.
- the third block corresponds to the PMT amplifier. I referred to the noise level after this section as N_{END}.

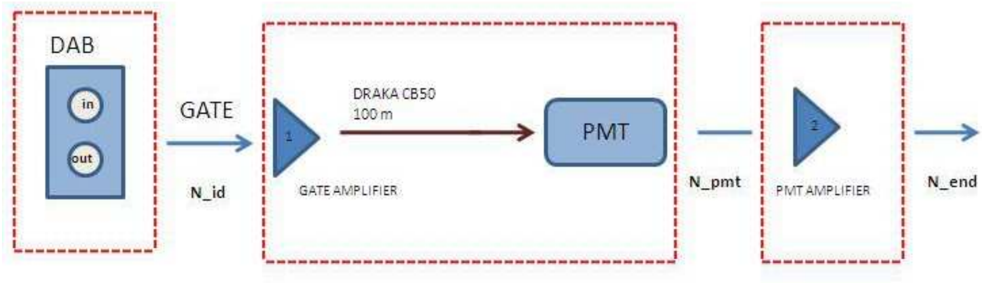

Figure 4.19: Testing setup for noise analysis

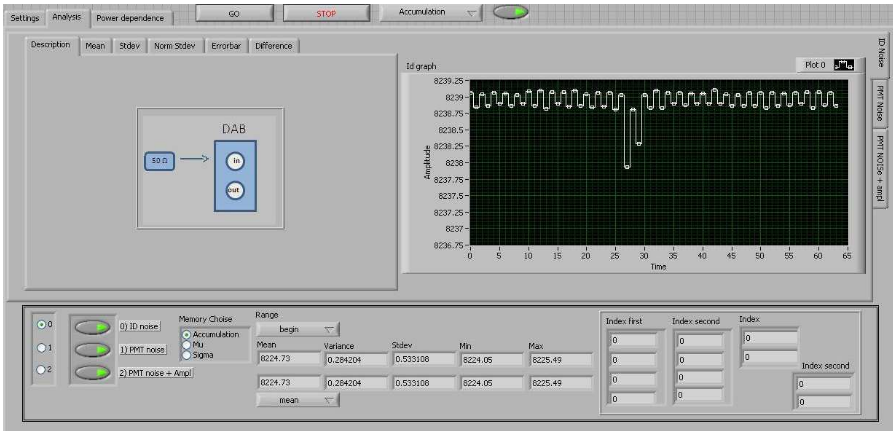

Figure 4.20: The noise analysis tool

The average and the standard deviation values of the measured noise data can be determined using two methods: via hardware (reading the values stored in the *Mu* and *Sigma* memories) and via software. The second modality was introduced in order to verify the FPGA algorithm which calculates these statistical values.

4.2.3.2 The noise analysis tool

I developed a LabVIEW tool to perform the described noise analysis. My program can (see figure 4.20):

- visualize the output data;
- determine all the statistical values, via hardware and software and compare them;

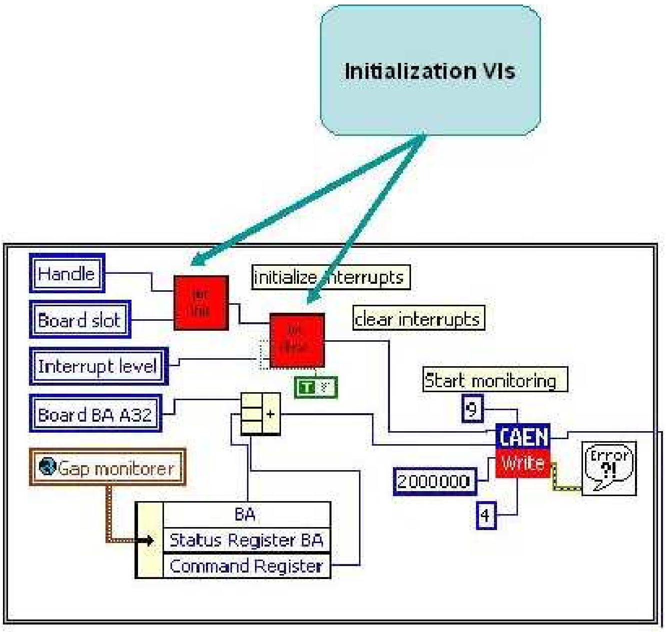

Figure 4.21: *Start Monitoring* Task: Initialiation VIs

- show the level of the noise in correspondance of the three sections of the testing setup chain mentioned above.

With my tool I realized these noise measurments as described in chapter 4.3.2.

4.2.4 Software maintenance and further developments

In order to make my software maintenance easier, as well as its reading and further developments, I applied some rules. I identified the basic functions and I developed dedicated Vis for them. I also implemented two specific subVIs for the noise analysis and the pulse delay generator control (see figure 4.6). Moreover I used different colours to classify all the VIs on the basis of their functions:

- red: initialiation VIs (figure 4.21);
- green: VIs responsible for data storage in files and folders (figure 4.22);
- orange: VIs responsible for generation of graphs (figure 4.23);

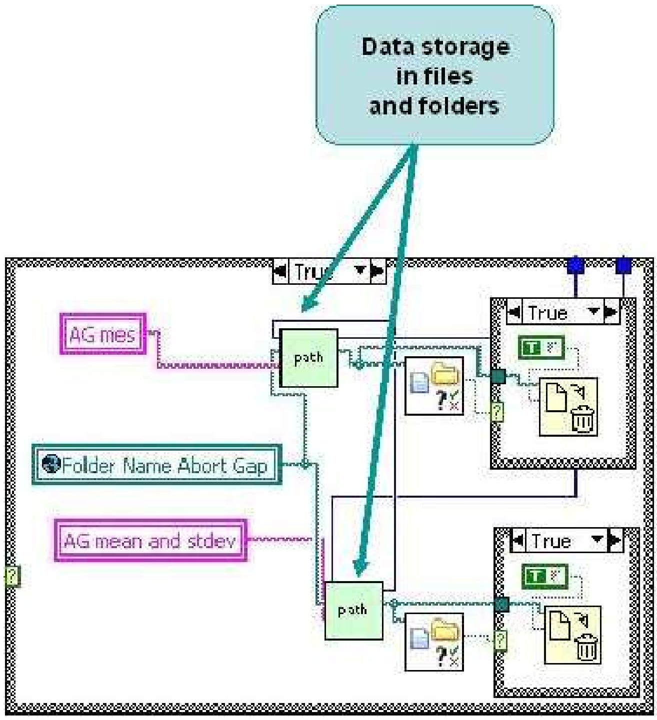

Figure 4.22: *Start Monitoring* Task: VIs responsible for data storage in files and folders

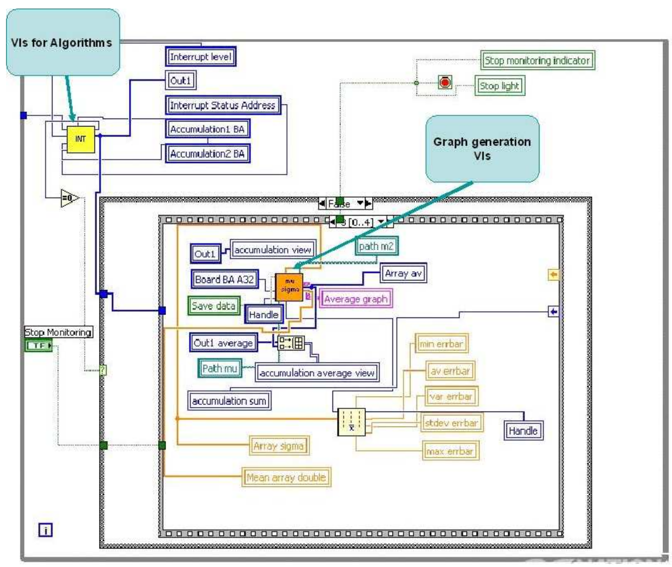

Figure 4.23: *Start Monitoring* Task: VIs responsible for generation of graphs and for the signal analysis or for other algorithms

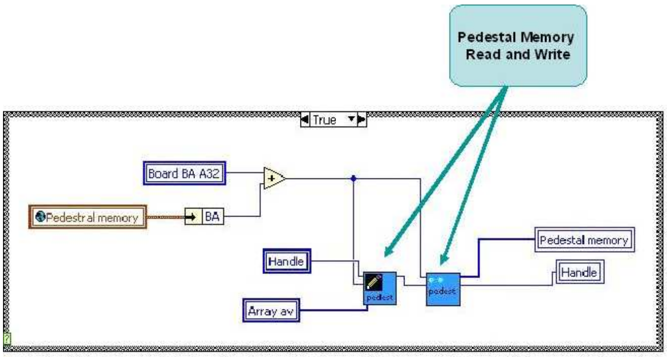

Figure 4.24: *Start Monitoring* Task: VIs responsible for reading data from internal memories

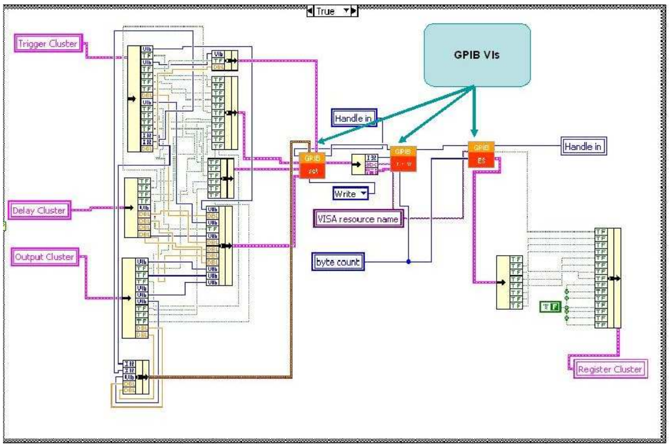

Figure 4.25: VIs responsible for the remote control of the pulse delay generator using the GPIB interface

- yellow: VIs responsible for the signal analysis or for other algorithms (figure 4.23);
- blu: VIs responsible for reading data from internal memories and registers (figure 4.24).

I used a dark shade for the principle VIs and a clear shade for the auxiliary ones.

I also used a different layout for the VIs responsible for the remote control of the pulse delay generator using the GPIB interface (see figure 4.25).

I introduced an online help in the most complicated VIs. I also decided to use txt files to store the measured data because this format is widely accepted

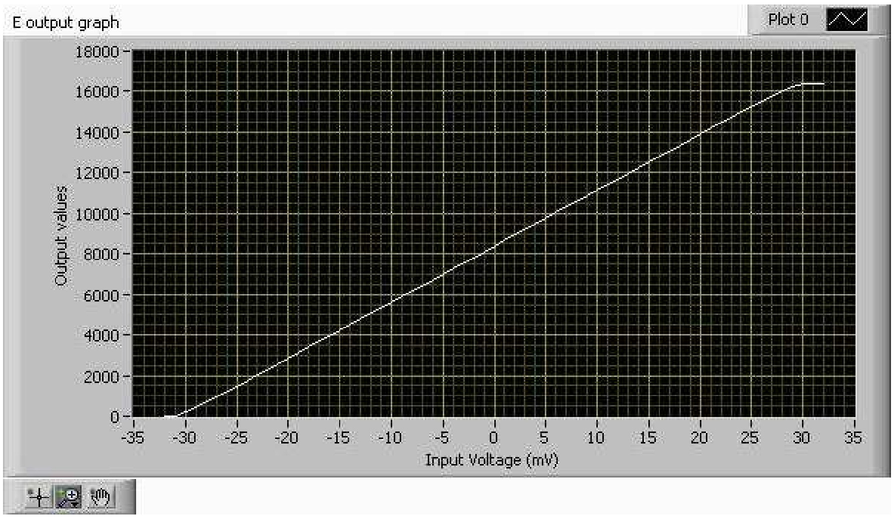

Figure 4.26: Integrator 0: I/O characteristic

among several systems.

4.3 Measurement and calibration

4.3.1 IBMS Integrator Calibration: Mezzanine 419

I calibrated the two integrators of one of the IBMS Mezzanines (419) using my software tool as described in 4.2.2. I progressively increased the input voltage from -32 mV to 32 mV with a step of 1 mV. This way, I determined the two integrators characteristics.

As we expected, the two integrators are not fully linear and their gains and offsets are not equalized, as shown in figure 4.28. The saturation points for these integrators are different: one of them, referred to as *integrator 0*, saturates for input voltage less or equal than -31 mV and greater or equal than 30 mV (see figure 4.26); the other one (*integrator 1*) saturates for input voltage less-equal than -31 mV and it does not saturate until 32 mV (see figure 4.27).

I calculated the gain - offset pairs (see figure 4.29) in correspondance of each *sample range* (the calibration procedure is described in chapter 4.2.2.1).

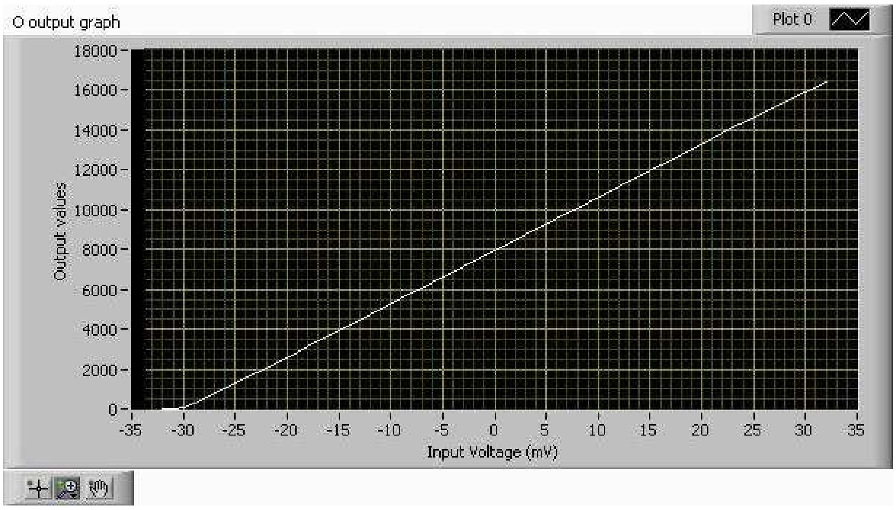

Figure 4.27: Integrator 1 : I/O characteristic

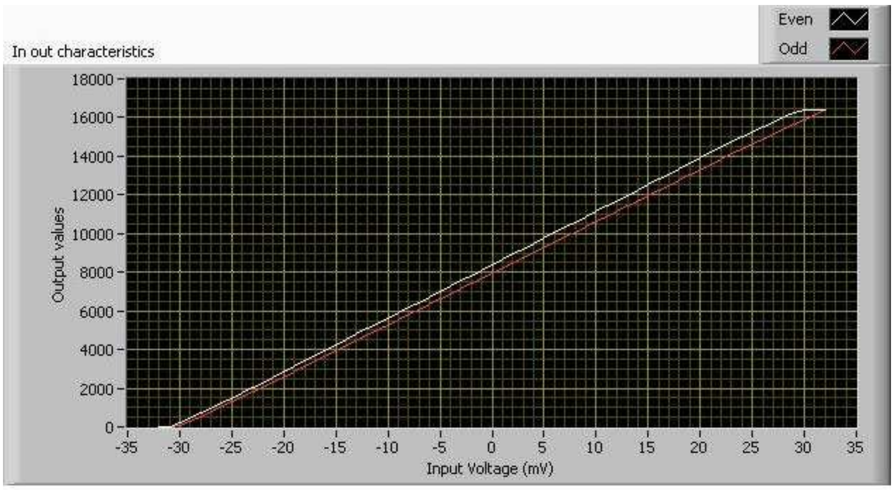

Figure 4.28: Comparison between integrato I/O characteristics

Sample Range	Gain	Offset
1	1,034542595	160,2910517
2	1,036547542	144,448588
3	1,037010468	140,8395549
4	1,036891955	141,8119395
5	1,036623392	143,937679
6	1,036711236	143,2552795
7	1,036944485	141,4108913
8	1,037035368	140,5875633
9	1,03686701	141,856709
10	1,036805311	142,3806185
11	1,036637579	143,7826453
12	1,03643086	145,3438932
13	1,036239324	146,9036613
14	1,036144256	147,7312138
15	1,036113745	148,0389035
16	1,03599442	149,2200877
17	1,035761079	151,2567563
18	1,035554493	152,9491865
19	1,035327091	154,730878
20	1,035144812	156,1403743
21	1,034963254	157,4139049
22	1,034809856	158,4538966
23	1,034670918	159,1703145
24	1,034463615	160,2192254
25	1,034265039	161,0505952
26	1,03402184	162,0892843
27	1,033768091	163,0260054
28	1,033497628	163,9308929
29	1,033211895	164,7690823
30	1,03212817	169,8322667
31	1,030592964	172,3015004
32	1,028015047	180,0131205

Figure 4.29: Gain and offset for eanch sample range

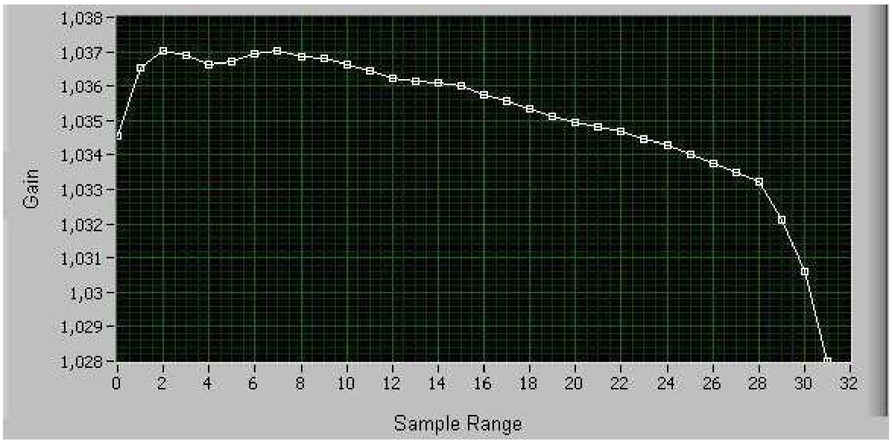

Figure 4.30: Gain values for each sample range

As we expected, gain values calculated for sample ranges greater than 28 can be ignored because for these voltage input values the integrators characteristis are strongly non linear (see figure 4.30): therefore I limited the range of the input voltage between -25 mV and 25 mV (figure 4.31).

My analysis has shown that sample ranges between 2 and 17 give best performances in the central part of the input voltage range - between -15 mV and 15 mV whereas sample ranges between 18 and 25 and sample range 1 give best performance in the ending part of the input voltage range - between -25 mV and -15 mV and 15 mV and 25 mV (see figure 4.32).

Since we are more interested in linearizing the integrators characteristics in the central part of the input voltage range, I selected the gain - offset pair correspondent to sample range 16: the maximum relative (to the measured value) square error in the central part of the input voltage range is equal to 0.64%; if we extend the range until 20 mV, the maximum relative square error increases until 2.25%, but this error is compatible with CERN specification. The selected gain and offset are respectively **1.03599442** and **149.2200877**.

4.3.2 Noise Measurements

As shown in figure 4.19, I measured noise levels in correspondance of three differents sections of my acquisition chain, as described in chapter 4.2.3. The

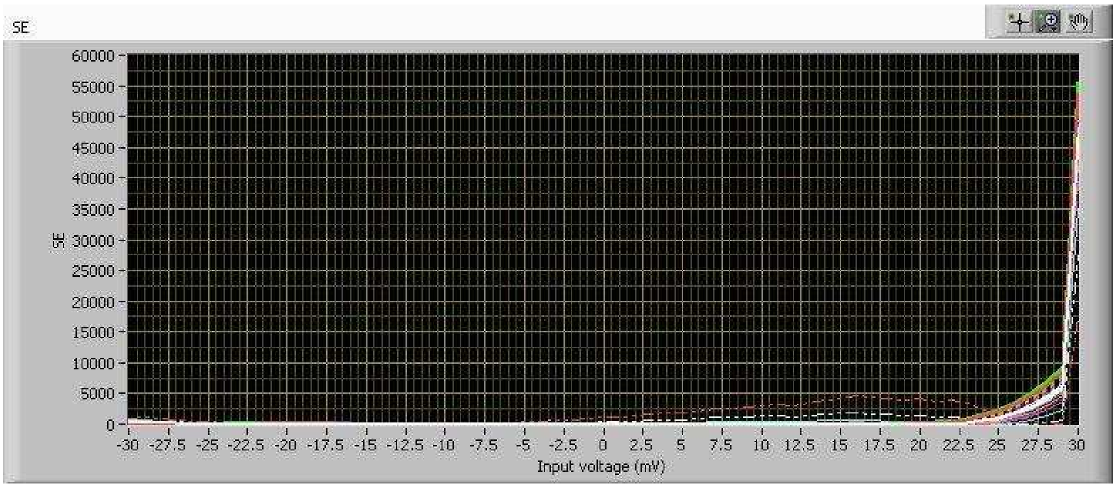

Figure 4.31: Square errors (y-axis, LSB) versus Input voltage (x-axis, mV)

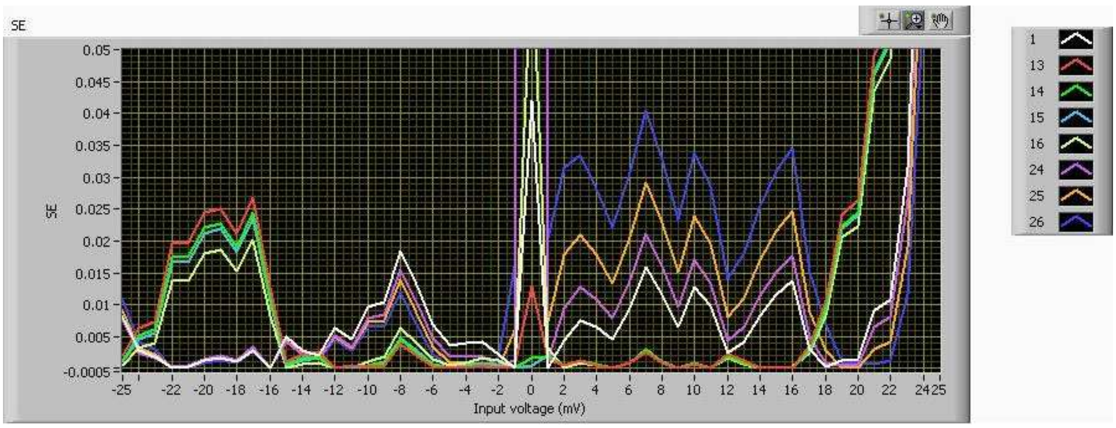

Figure 4.32: Relative square error % versus Input voltage (-25mV : 25 mV)

Measurement Parameters	
Mezzanine	419
Gate length	60 bcp = 1.5µs
Observation period	2000
Tckl – Gate Delay	0 bcp
Gate – Acquisition Delay	0 bcp
IIR band	2 Hz
HVPS	0kV

Figure 4.33: Setting values for the FPGA controls (*bcp*: bunch clock period; *HVPS*: High Voltage Power Supply)

second goal of my analysis is to verify the FPGA algorithm responsible for calculating the statistical values.

The maximum difference between the average of the measured noise values calculated via hardaware and the ones calculated via software is less than 1.2 LSB (0.57 %) (see figure 4.34); this value increases to 18 LSB (8.76%) for the standard deviation values (figure 4.35). These differences depend on the small number of measurements (120) used to calcultate these statistical values via software: I tryed to increase this number until 1000 and the differences decreased until less than 1 LSB. I can conclude that the FPGA algorithm used to calculate average and standard deviation of the measured values gives consistent results.

I measured the average and the standard deviation of the measured data in correspondance of three differents sections of my acquisition chain (see figure 4.36): in order to give an estimation of the performance of our system, I calculated the ENOB (Effective Number of Bits) of our system. This values described the actual dynamic range of the system.

The ENOB values in correspondance of the first and of the second sections are respectively 10.57 and 10.5608: I can conclude that the second section (gate

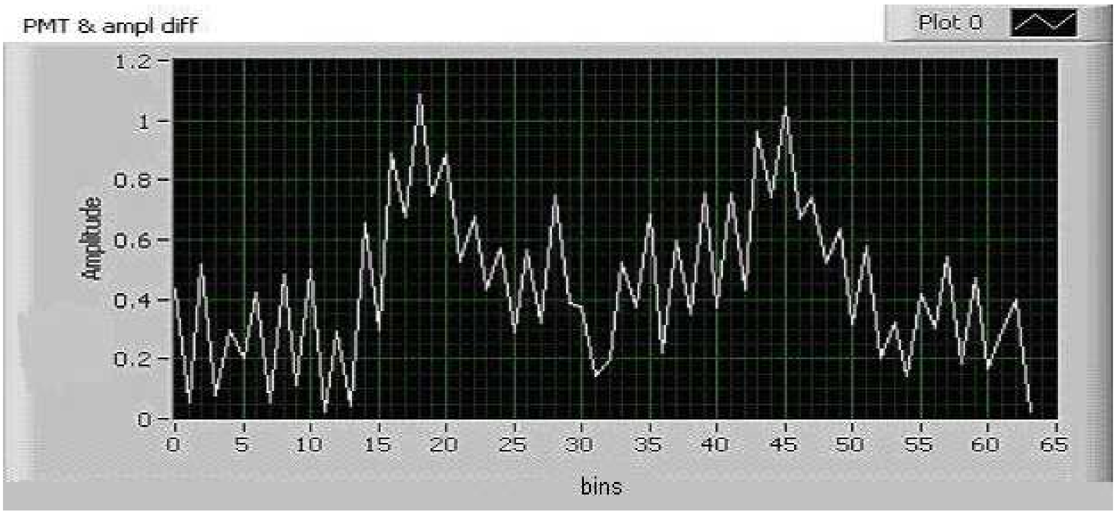

Figure 4.34: Difference between average of measured values calculated via hardware and software

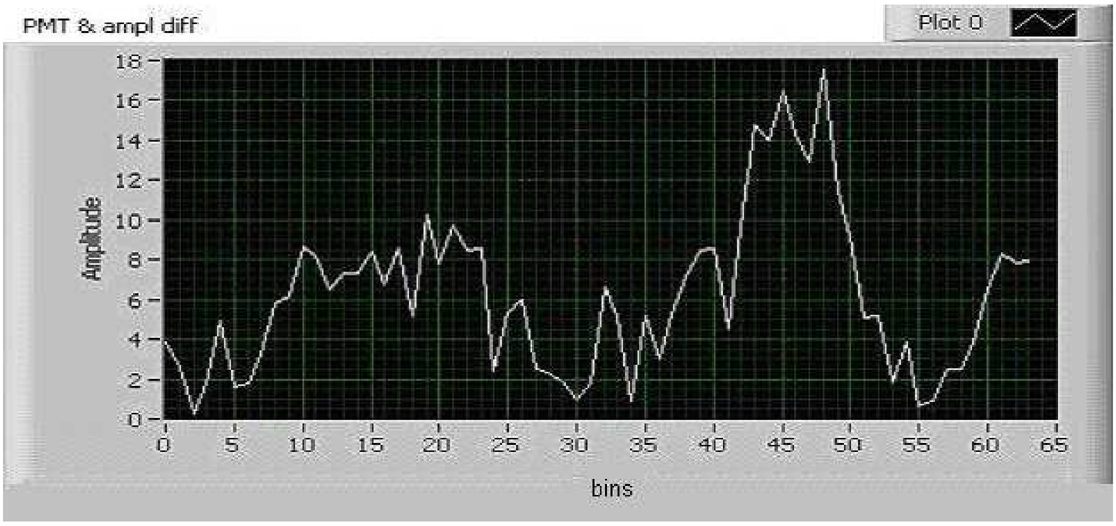

Figure 4.35: Difference between standard deviation of measured values calculated via hardware and software

		Mean Output Value	Standard Deviation
ID Noise	Mean	8238.5	8.82608
	Min	8237	8.718
	Max	8239.98	8.944
PMT Noise	Mean	8226.41	8.8635
	Min	8225.01	8.718
	Max	8227.03	9
END Noise	Mean	8201.1	130.829
	Min	8171.14	129.838
	Max	8341.01	138.083

Figure 4.36: Noise levels resume

amplifier and cable, PMT) does not increase significantly the noise level. The most noisy element of the chain is the PMT amplifier: in fact the ENOB value at the end of the chain is equal to 6.68, but this level of noise is compatible with CERN requirements, taking also in consideration that the dynamic range can be increased by optic filters and high voltage settings.

Moreover I compared my results with the ones obtained from the setup installed in the LHC tunnel: the results are consistent (see figure 4.37).

4.3.3 Dependency of the response on the position of the light pulse inside the gate

I measured the amplitude of the output signal coming from the PMT moving its position inside the gate, in order to verify if it is constant or if there is a relationship between the amplitude value and the position of the pulse with respect to the gate. To realize these measurements I used my software, described in chapter 4.2.1.

I performed my measurements by changing these parameters (see figured 4.38, 4.39 and 4.40):

- the delay A of the pulse delay generator, in order to change the position of the pulse with respect to the gate signal;

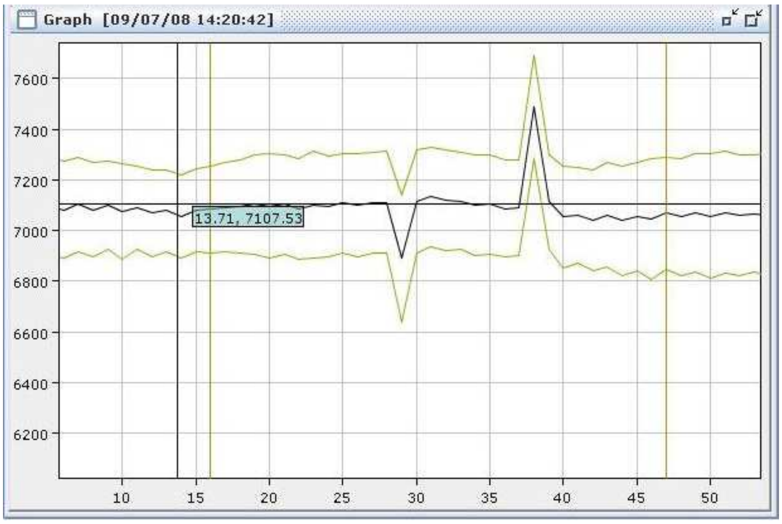

Figure 4.37: Average and Standard deviation of measured data from the setup installed in the LHC tunnel: the green curve represents the standard deviation values; the black one the data averages. The two peaks are in correspondence of the start and the end of the gate signal.

FPGA Parameters	
Gain 0	1
Gain 1	1.03599
Offset 0	149
Offset 1	0
Observation Period	2000
Tclk-gate delay	10
Gate- acquisition delay	20
IIR band	0.05
ADC clk phase	1
Cycle Number	120

Figure 4.38: FPGA parameter settings

Instrumentation Parameters	
High Voltage Power Supply	-2,40 kV
Filter	1.0
Photodiode – PMT distance	6,054 cm

Figure 4.39: Instrumentation settings

Pulse Delay Generator Parameters	
Trigger	Ext, 0.5V, positive slope, 50 ?
Delay C	0 ns
Delay D	1 ns
Output T0	50 ohm, TTL, polarity = Normal
Output A	50 ohm, TTL, polarity = Normal
Output B	High, TTL, polarity = Normal
Output AB	50 ohm, TTL
Output C	High, TTL, polarity = Normal
Output D	High, TTL, polarity = Normal
Output CD	High, TTL

Figure 4.40: Pulse delay generator settings

- the delay B of the pulse delay generator, in order to change the pulse width;
- the presence or less of the coaxial cable which connects the gate amplifier to the PMT in the setup shown in figure 4.1.

I verified that the rise and the fall time of the photodiode are almost 50 ns: I performed my measuremnts with a pulse width of 50 ns (see figure 4.41).

I measured the amplitude values of the output signal moving the pulse inside the gate with a step of 10 ns: since the resolution of the Accumulation Memory is 100 ns, we can see a periodicity of 10 samples (see figure 4.42).

The large variability of the signal amplitude (figure 4.42) depends on the dead time present in the system due to the switching between the two integrators of the mezzanine (see chapter 3). The weight of the not - integrated part of the pulse depends on the phase relation between its position and the sampling clock, linked with the 100 ns - periodicity. Monitoring the amplitude pulse value

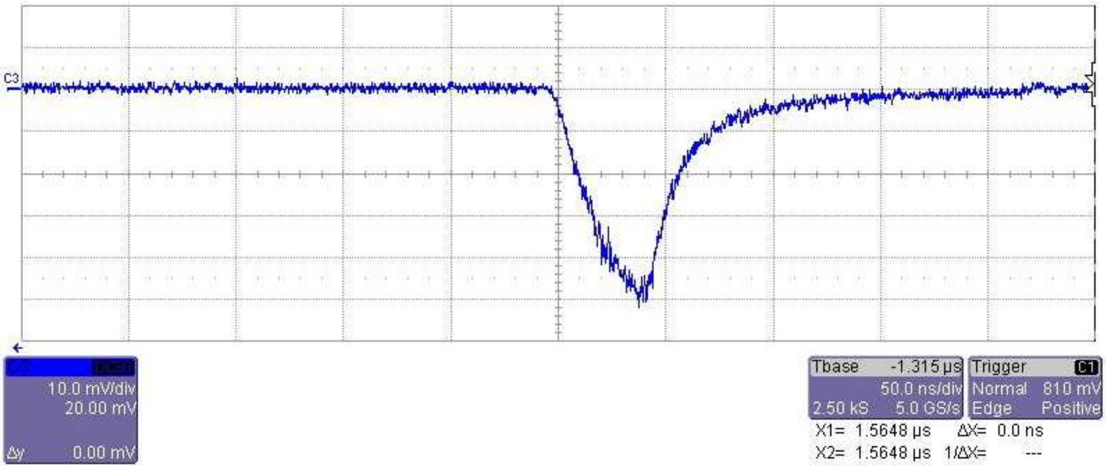

Figure 4.41: Output pulse form oscilloscope -pulse width: 50 ns, delay A: 1560 ns

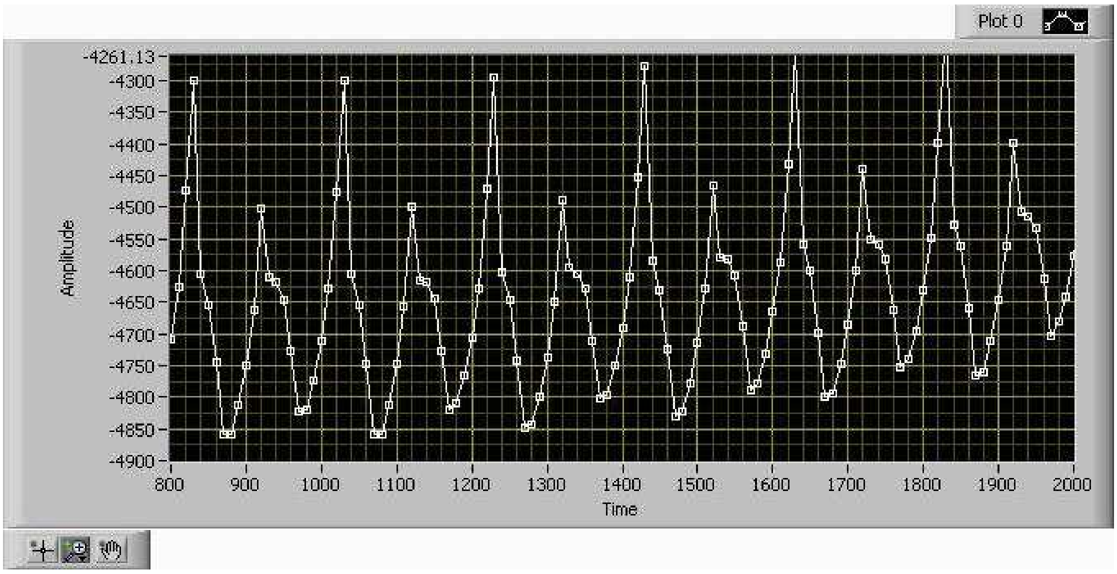

Figure 4.42: Pulse Amplitude scan: 3-sample integration; delay A from 3000 ns to 1 ns with step of 10 ns

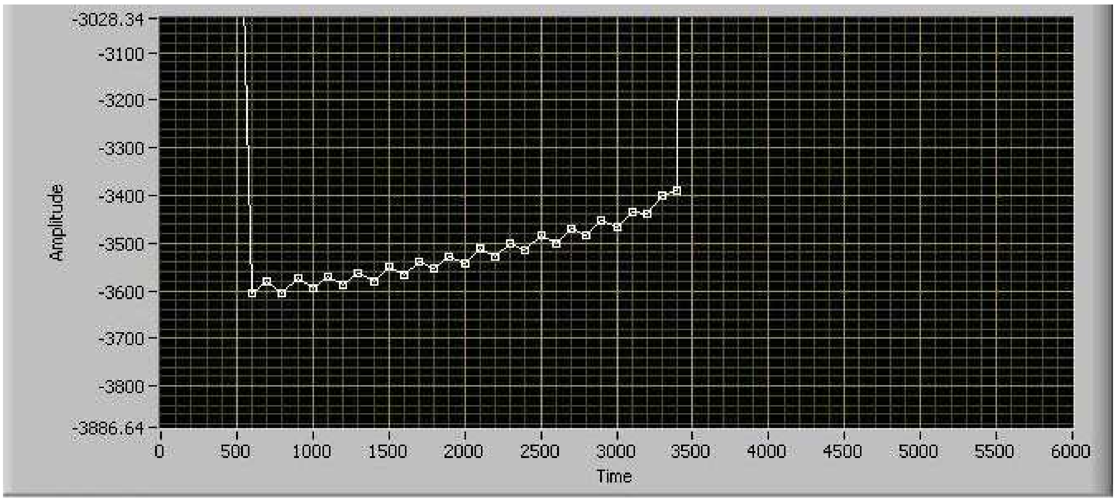

Figure 4.43: Pulse Amplitude scan: delay A from 6000 ns to 1 ns with step of 100 ns

and doing an accumulation on 3 samples I can obtain a 12.8% variation of the measured signal value.

To remove these artificial effects, also due to the pulse shape (see figure 4.41), I performed the rest of my analysis moving the pulse inside the gate with steps equal to 100 ns. Other two can effects can be observed:

- the alternance of the measured amplitude values (figure 4.43) depends on the residual difference between the offsets of the two integrators characteristics.

- Moving the pulse with respect to the gate, the variation of its amplitude is equal to 5.9% (almost 200 LSB): this variation depends with great probability on the gate shaping. In fact, I repeated the measurements introducing the coaxial cable which carries the gate signal to the PMT and this shaping effect is more evident (see figure 4.44).

In this second case, in fact, the pulse amplitude variation is 6.3%. However these variations are perfectly compatible with CERN requirements (50% of accuracy).

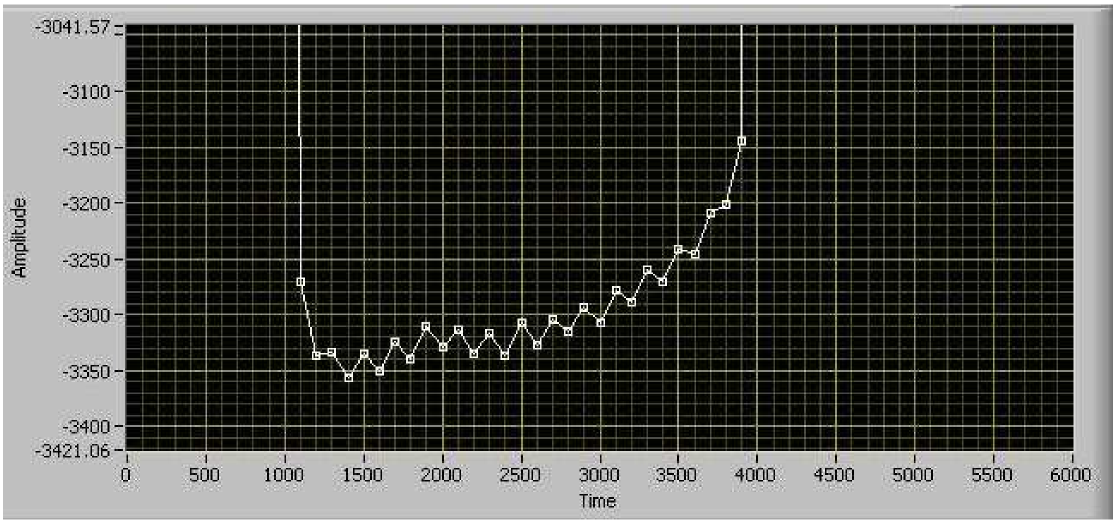

Figure 4.44: Pulse Amplitude scan: delay A from $6000\ \mathrm{ns}$ to $1\ \mathrm{ns}$ with step of $100\ \mathrm{ns}$

4.3.4 Hysteresis

In order to verify if the system has hysteresis with respect to the high voltage power supply, I measured the amplitude of the output pulse by varying the voltage input value coming from the high voltage power supply from $-1.90\ \mathrm{kV}$ to $-3.00\ \mathrm{kV}$ and vice versa (figures 4.45, 4.46 and 4.47).

A difference between the two curves was indeed observed: its maximum value is equal to 2% (figure 4.48). I could not digitally control the high voltage power supply: the difference from the set values can be considered in the same order of magnitude as the measurement error. I can conclude that the system does not show a measurable hysteresis with respect to the high voltage power supply.

FPGA Parameters	
Gain 0	1
Gain 1	1.03599
Offset 0	149
Offset 1	0
Gate Length	60
Observation Period	2000
Tclk-gate delay	4
Gate- acquisition delay	20
IIR band	0.05
ADC clk phase	1
Cycle Number	120

Figure 4.45: FPGA parameters settings

Instrumentation Parameters	
High Voltage Power Supply	-1.90 : -3.10 kV step 0.01 kV
Filter	2.0
Photodiode – PMT distance	6,054 cm
Pulse width	20 ns

Figure 4.46: Instrumentation parameters settings

Pulse Delay Generator Parameters	
Trigger	Ext, 0.5V, positive slope, 50 Ohm
Delay A	850ns
Delay B	20 ns
Delay C	0 ns
Delay D	1 ns
Output T0	50 ohm, TTL, polarity = Normal
Output A	50 ohm, TTL, polarity = Normal
Output B	High, TTL, pdarity = Normal
Output AB	50 ohm, TTL
Output C	High, TTL, pdarity = Normal
Output D	High, TTL, pdarity = Normal
Output CD	High, TTL

Figure 4.47: Pulse delay generator parameters settings

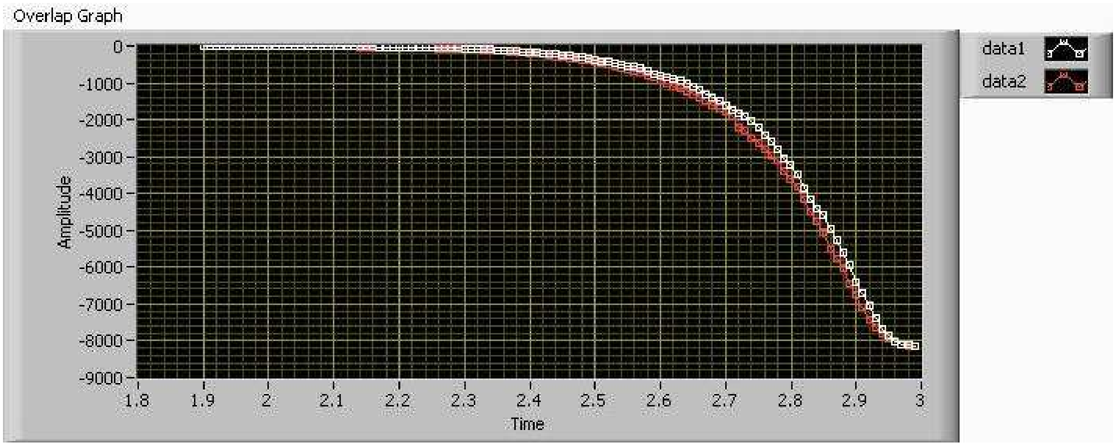

Figure 4.48: Pulse amplitude curves: data 1 for input voltage from -1.9 kV to -3 kV; data 2 for input voltage from -3 kV to -1.9 kV

Chapter 5

Conclusion

My project is made up of two sections, one for each theme analyzed during this year at CERN: the first one concerns the Tune, the second one is about the Abort gap.

As for the tune, the goal of my project was to test the post mortem memory of the DAB. In order to do it, I developed a LabVIEW software as an interface to this memory and I performed some tests properly simulating events of beam loss. At the same time I understoond the basic concepts about the tune measurements and I familiarized with the standard AB - BI tool of istruments.

The second part of my project is about the abort gap. In this framework, my tasks consisted in:

- to allow the user to monitor the abort gap, developing a software application to interface with the FPGA responsible for the data processing.
- to develop a testing setup to verify the synchronization procedure with the FPGA and the performance of the acquisition chain.
- to calibrate the system and to analyze its performance (signal-noise ratio), in order to compare my results with the ones coming from the same setup located in the tunnel of LHC.

The obtained results can be summerized as follows:

- The testing setup is fully working and reproduces the one located in LHC tunnel. I interfaced with it using my applications developed in LabVIEW.
- I calibrated the integrators of the mezzanine 419: their parameters show a well correlated temperature dependance. For this reason it will be necessary to recalibrate them periodically.
- About the noise in the system, the most noisy element is the PMT amplifier: the ENOB value measured at the end of the chain is equal to 6.68. I can conclude that the performance of the system is good and the noise does not represent a problem.
- I analyzed the dependence of the amplitude of the system output signal on its position with respect to the gate. The maximum variation of the output signal amplitude obtained is equal to the 6% of the measured amplitude value and it is greatly compatible with CERN requirement (50 % of accurancy).
- I veryfied that the system does not have a measurable hysteresis.

About further developments:

- It could be important to verify with more tests the dependence of the gains and offset of the mezzanine integrators on the temperature and to develope a system to self-calibrate them.
- I calibrated other mezzanines and I noticed big differences between the performances of the chips.
- It is important to repeat these tests with the setup located in LHC tunnel because the environment is different from the one in the laboratory.

Appendix A

How to run my software tools

All my software applications use the functions of the CAENVMELib.

A.1 Software to test the Post Mortem memory

All the necessary VIs are in the folder ”post mortem”. When the user opens this folder, he has to run the file ”main”.

A.2 Abort Gap Main Tool

All the necessary VIs are in the folder ”abort gap monitorer”. When the user opens this folder, he can find a folder ”ATOMS”which contains all the subVIS and a file ”AGmain”: this the file that has to be run. All the files generated by my program are saved in a folder ”C: \ Abort gap”.

A.3 Calibration Tool

All the necessary VIs are in folder ”calibration”. When the user opens this folder, he can find a folder ”ATOMS”which contains all the subVIS and a file ”CAL MAIN”: this the file that has to be run. All the files generated by my program are saved in folder ”C: \ gain and offset range”.

A.4 Noise Analysis Tool

All the necessary VIs are in folder ”abort gap monitorer”. When the user opens this folder, he can find a folder ”ATOMS”which contains all the subVIS: one of them is ”NOISE ANALYSIS”. The user has to run this one. All the files generated by my program are saved in folder ”C: \ Abort gap”.

Bibliography

[1] Edmund Wilson "An Introduction to Particle Accelerators",CERN Accelerator School, Geneva.

[2] Rohlf, James Williams "Modern physics from A to Z0", Wiley, 1994.

[3] Jackson John D. "Classical Electrodynamics", 3rd edition, Wiley, 1998.

[4] J. Rossbach, P. Schmuser"Basic Course On Accelerator Optics".

[5] D.A. Edwards, M.J. Syphers. "An Introduction to the Physics of High Energy Accelerators", Wiley-VCH 2004.

[6] A. Boccardi, M.Gasior, O.R.Jones, K.K.Kasinski, R.J. Steinhagen"The FPGA-based continuous FFT tune measurement system for the LHC and its test at the CERN SPS", CERN, Geneva, Switzerland.

[7] M.Gasior, R. Jones "The Principle and the First Results of Betatron Tune Measurement by Direct Diode Detection", in *LHC-Project Report 853*, Geneva, Switzerland, August 2005.

[8] Andrea Boccardi "DAB64x Stratix FPGA for tune measirements", in Notes, CERN 2007.

[9] C. Fischer "LHC-B-ES-0005", in LHC specification, CERN 2003.

[10] R. Jones "The CERN Beam Instrumentation Digital Acquisition Board (DAB64x) - Tune Feedback Review", in BNL, CERN April 2005.

[11] VME web page`http:http://www.interfacebus.com/`.

[12] Hamamatsu Photonics KK. “Photomultiplier Tubes. Basics and Applications”, Hamamatsu, 2006.

[13] CERN home page. http://user.web.cern.ch/user/Welcome.asp.

[14] AB-BI-QP home page. http://ab-dep-bdi-em.web.cern.ch/.

Acknowledgements

I would like to thank Andrea Boccardi for his great help in every situation. Special thanks also to Thibaut Lefevre for all the time he dedicated to me. I am very grateful to my professors Gianluca Mazzini, Gianluca Setti and Velio Tralli for their help and to have given me the possibility to live this experience. Thanks to all the AB-BI-QP section members for their constant help.

I am really grateful to my old and new friends: Alessandro, David, Clara, Maria.

Really thanks to Pablo, David, Sulveig, Katrine, Odd, Natalie, Berta, Martin, Sandro, Pauline, Manu, Juan, Edu, Giacomo, Simone, Alex, Adriana, Fabio, Sonia, Laura and Vincenzo.

Finally thanks to my parents for their help.

Scritta con $\LaTeX\,2_\varepsilon$ e BibTeX

Stampata il July 17, 2008